Research Square

Preprints are preliminary reports that have not undergone peer review.
They should not be considered conclusive, used to inform clinical practice,
or referenced by the media as validated information.

Bidirectional host–microbe signaling through cortisol metabolism by the gut bacterium Agathobaculum desmolans

Maayan Freiberg
University of Illinois at Urbana-Champaign
Francelys V Fernandez-Materan
University of Illinois at Urbana-Champaign
Taojun Wang
University of Illinois at Urbana-Champaign
Lindsey K. Ly
University of Illinois at Urbana-Champaign
Margaret Abernathy
University of Illinois at Urbana-Champaign
Pius Sarfo Buobu
Purdue University
Sarah Goldberg
University of Illinois Chicago
Lucille Ray
University of Illinois Chicago
Alyshia Hamm
University of Illinois Chicago
Nicollette Kessee
University of Illinois Chicago
Hanchu Dai
University of Illinois at Urbana-Champaign
Ece Mutlu
University of Illinois Chicago
Steven L. Daniel
University of Illinois at Urbana-Champaign
Sage J. Kim
University of Illinois Chicago
Paul Grippo
University of Illinois Chicago
Patricia G. Wolf

Purdue University

Lisa Tussing-Humphreys

University of Illinois Chicago

H. Rex Gaskins

University of Illinois at Urbana-Champaign

Andrew J. Steelman

University of Illinois at Urbana-Champaign

Jason M. Ridlon

jmridlon@illinois.edu

University of Illinois at Urbana-Champaign

Article

Keywords:

Posted Date: November 12th, 2026

DOI: https://doi.org/10.21203/rs.3.rs-11445266/v1

License: This work is licensed under a Creative Commons Attribution 4.0 International License.
Read Full License

Additional Declarations: No competing interests reported.

Bidirectional host–microbe signaling through cortisol metabolism by the gut bacterium *Agathobaculum desmolans*

Maayan Freiberg[a,b], Francelys V Fernandez-Materan[a,b], Taojun Wang[a,b,c], Lindsey K. Ly[a,b], Margaret Abernathy[a,b], Pius Sarfo Buobu[d], Sarah Goldberg[e], Lucille Ray[e], Alyshia Hamm[e], Nicollette Kessee[e], Hanchu Dai[a,b,f], Ece Mutlu[e], Steven L. Daniel[b], Sage J. Kim[g], Paul Grippo[e], Patricia G. Wolf[d], Lisa Tussing-Humphreys[h], H. Rex Gaskins[a,b,i], Andrew J. Steelman[a,b,i,j], Jason M. Ridlon[a,b, i,k]

[a]Carl R. Woese Institute for Genomic Biology, University of Illinois at Urbana-Champaign, Urbana, IL, USA;

[b]Department of Animal Sciences, University of Illinois at Urbana-Champaign, Urbana, IL, USA;

[c]Present address: Department of Nutrition and Health, China Agricultural University, Beijing, China.

[d]Department of Nutrition Science, Purdue University, West Lafayette, IN, USA.

[e]Department of Medicine, University of Illinois Chicago, Chicago, IL, USA.

[f]Present address: Department of Biochemistry, University of Illinois Urbana-Champaign, Urbana, IL, USA.

[g]Department of Health Policy and Administration, University of Illinois Chicago, Chicago, IL, USA.

[h]Department of Kinesiology and Nutrition, University of Illinois Chicago, Chicago, IL, USA.

[i]Division of Nutritional Sciences, University of Illinois at Urbana Champaign, Urbana, IL, USA;

[j]Neuroscience Program, University of Illinois Urbana-Champaign, Urbana, IL, USA.

[k]Cancer Center at Illinois, Urbana, IL, USA;

*Corresponding author: Jason M. Ridlon; jmridlon@illinois.edu

ABSTRACT

Microbial endocrinology has developed principally around bacterial metabolism of catecholamines, yet the intestinal lumen receives far larger quantities of host steroids. Here we characterize cortisol metabolism by *Agathobaculum desmolans* ATCC 43058 as a model for the HPA axis arm of this interaction. Cortisol elicited extensive transcriptional remodeling, dominated by induction of the steroid-17,20-desmolase pathway but extending to motility, sporulation, and mobile genetic elements. Recombinant DesAB preferentially cleaved cortisol and displayed substrate-specificity distinct from *Clostridium scindens* DesAB. Its product, 11β-hydroxyandrostenedione, is a precursor of 11-oxygenated androgens that agonize the nuclear androgen receptor; in primary mouse intestinal cells it induced MAPK, cytokine, and cell-adhesion programs and altered VCAM1, CSF1, CSF1R and IGFBP6 abundance. Bacterial cortisol metabolism therefore transforms a host glucocorticoid signal into an androgenic one, establishing the sterolbiome as a mechanistically tractable arm of microbial endocrinology.

INTRODUCTION

From the first hormones described to the receptors discovered decades later, endocrinology has grown by following function wherever it leads - across chemical classes, across tissues, and, a growing body of work suggests, across kingdoms. Steroids, bile acids, thyroid hormones, and peptides are recognised as hormones not because they share a common structure but because they meet a functional criterion: they are produced at one site, act at another, and alter cellular response through defined receptors. The field of microbial endocrinology, established on the recognition that bacteria both produce and respond to host hormones that coordinate host physiology (Lyte, 2016), has developed principally around the catecholamines. Yet the criterion that admits catecholamines has clear parallels among other hormones, including steroids that also reach the intestinal lumen.

Cortisol is a major glucocorticoid coordinating the mammalian response to physiological and psychological stress. The metabolism of cortisol offers a direct test of this framework. A small number of bacteria isolated from the human intestinal and urinary microbiomes cleave cortisol's C17 side-chain via the steroid-17,20-desmolase (DesAB) pathway, generating 11β-hydroxyandrostenedione (11β-OHAD) (Ly et al., 2020; Ridlon et al., 2013; Wang et al., 2025). Both mammalian tissues and members of the microbiota possess enzymatic activities capable of further metabolising 11β-OHAD into 11-oxygenated androgens (Barnard et al., 2018; Pretorius et al., 2016; Schiffer et al., 2018; Wang et al., 2025), so that microbial side-chain cleavage has the potential to redirect a host glucocorticoid into a distinct class of signalling steroids that agonizes the host nuclear androgen receptor.

Bacterial catecholamine and 11β-OHAD production proceeds by the same logic. Decarboxylation of host and diet-derived tyrosine or DOPA yields a bioactive amine while returning carbon and nitrogen to the cell, so that a single enzymatic step serves both bacterial metabolism and host signalling (Sie & Tropini, 2026). Side-chain cleavage of cortisol is

directly analogous: the released two-carbon unit may be assimilated by the bacterium, while the remaining steroid nucleus is a distinct, biologically active molecule returned to the host.

Two features qualify a system for this framework, and the gut microbiota satisfy both for steroids. The first is enzymatic transformation. The sterolbiome, the collective steroid-metabolising capacity of the gut microbiota, is defined in the same terms endocrinology has always used for steroid biotransformation: specified reactions, characterised enzymes, and identified genes (Ridlon, 2020). As with bacterial catecholamine production, this transformation does not require the bacterium to possess the receptor through which its product acts: dopamine receptors and the nuclear androgen receptor are both eukaryotic innovations with no bacterial counterpart, so in each case the converting organism and the responding cell are necessarily distinct. The second feature is that the transformation is coupled to a response in the transforming cell: steroids and bile acids elicit distinct transcriptional programs in the gut bacteria that metabolise them (Devendran et al., 2019; Ridlon et al., 2013; Wylensek et al., 2020), the same criterion by which catecholamine responsiveness qualified those molecules for the field. Elucidating the sterolbiome is therefore important for the advance of both classical and microbial endocrinology alike.

The genetic basis for microbial cortisol side-chain cleavage was first defined in *Clostridium scindens* ATCC 35704, where cortisol-responsive transcriptomics identified a highly induced steroid-metabolism locus comprising *desC* (20α-hydroxysteroid dehydrogenase), *desA* and *desB* (the two subunits of steroid-17,20-desmolase), and *desD* (a putative transporter) (Devendran et al., 2018; Ridlon et al., 2013). Identification of *desAB* subsequently enabled recognition of homologous pathways in other steroid-metabolising bacteria, including *Agathobaculum desmolans* ATCC 43058 and *Clostridium cadaveris*. In contrast to the 20α-HSDH activity of *C. scindens*, *A. desmolans* and *C. cadaveris* possess 20β-HSDH activity, generating 20β-dihydrocortisol (Bokkenheuser et al., 1986; Devendran

et al., 2017) evidence that phylogenetically distinct cortisol-metabolising bacteria have evolved related but biochemically differentiated pathways.

Homologues of *desAB* also occur in bacteria not historically associated with steroid metabolism, including the intestinal isolate *Intestinibacillus* sp. Marseille-P4005 and the urinary tract isolates *Propionimicrobium lymphophilum* and *Arcanobacterium urinimassiliense (Ly et al., 2020)*. The occurrence of cortisol side-chain cleavage across intestinal and urinary microbiomes, and its capacity to convert endogenous or pharmaceutical glucocorticoids into androgen precursors (Wang et al., 2025), raises the possibility that microbial glucocorticoid metabolism has biological consequences extending well beyond bacterial steroid catabolism. Whether cortisol acts as an environmental signal that alters the physiology of cortisol-metabolising bacteria, and whether the resulting metabolites in turn alter host-cell physiology, remains poorly understood.

A. desmolans ATCC 43058 provides a particularly useful organism in which to examine these questions. Originally isolated from feline faeces as *Eubacterium desmolans*, it was distinguished by its ability to cleave the cortisol side chain (Bokkenheuser et al., 1986). It was subsequently reassigned to *Butyricicoccus (Takada et al., 2016)* and then *Agathobaculum* (Ahn et al., 2016). Despite this, comparatively little is known of its genome, physiology, or response to host-derived steroids, and the effects of 11β-OHAD, the immediate product of DesAB-mediated cleavage, on intestinal physiology have not been defined.

Here, we use cortisol metabolism by *A. desmolans* as a model system for the HPA arm of microbial endocrinology, an axis that, unlike the SAM/catecholamine arm, has remained largely uncharacterised at the mechanistic level. We characterised the genome and cortisol-responsive transcriptome of *A. desmolans* ATCC 43058, determined the kinetics and substrate specificity of its recombinant DesAB enzyme, and examined the transcriptional and protein responses of primary mouse intestinal cells to products of microbial cortisol

metabolism. We further quantified faecal *desA* abundance in a human cohort previously characterised for long-term cortisol exposure and neighbourhood-level environmental stressors. Together, these approaches test a model in which a host endocrine signal alters bacterial physiology and is, in turn, transformed by microbial metabolism into a metabolite capable of modifying host-cell signalling.

RESULTS

Genomic characterization of *A. desmolans* ATCC 43058

Long-read sequencing of *Agathobaculum desmolans* yielded a 2,761,597 bp assembly comprising two circular contigs. The chromosome was assembled as a single circular contig of 2,753,494 bp, with a mean read depth of approximately 36×, whereas the second contig measured 8,100 bp and had a mean read depth of 773×. Genome quality assessment using CheckM v1.1.9 estimated 98.66% completeness and 0.34% contamination. BUSCO v6.0.0 analysis identified 92.2% completeness, comprising 89.7% complete single-copy, 2.6% duplicates, 6.0% fragmented, and 1.7% missing. Flye assigned a multiplicity of 24 to the smaller contig, consistent with its substantially higher read depth and suggesting that it may be present at a higher copy number than the chromosome.

geNomad v1.12.0 (Camargo et al., 2024) classified the 8,074-bp contig as plasmid-like, with a plasmid-like element (chromosome_score 0.0024, plasmid score 0.9880; virus score 0.0096), and predicted 10 open reading frames (ORFs), none of which had an assigned function (**Supplementary Figure 1a**). However, MOB-suite v3.1.0 (Robertson and Nash, 2018) did not identify known plasmid-associated replication or mobilization markers. This negative result does not exclude a plasmid origin, given the limitations of reference-based plasmid typing for poorly represented bacterial groups. Thus, although the contig's circularity, elevated read depth, and geNomad classification are consistent with a candidate plasmid, its

biological identity remains unresolved and further characterization is needed before it can be conclusively identified as a plasmid (Supplementary Fig. 1).

Genome-based classification using GTDB-Tk v2.3.0 and GTDB release 226 placed the organism within the genus *Agathobaculum*, family *Butyricicoccaceae*, order *Oscillospirales*, and class *Clostridia*. Comparison with the *A. desmolans* ATCC 43058 reference genome (GCF_000701665.1) using FastANI v1.32 yielded 99.88% average nucleotide identity (ANI) across 89.86% of the query genome, supporting its identification as *A. desmolans* (**Supplementary Fig. 1b-c**). BLASTn analysis identified 3,819 alignments, of which 79 (approximately 2.1%) were at least 5 kb long. These longer alignments covered approximately 2.57 Mb (93%) of the assembled sequence and showed nucleotide identities above 99.99%. The longest alignments ranged from 76 to 125 kb, indicating extensive sequence similarity between the assembly and the reference genome.

Genome annotation identified 2,784 predicted protein-coding sequences, 12 rRNA genes, 66 tRNA genes, and one CRISPR locus on the chromosome-sized contig (**Fig. 1a**). Of these, 1,414 were annotated as hypothetical proteins. Functional classification using eggNOG-mapper assigned 722 genes to COG categories associated with metabolism, 619 to information storage and processing, and 452 to cellular processes and signaling, whereas 731 were poorly characterized or lacked a defined COG assignment (**Fig. 1b**). The *desEAB* genes harbor a downstream *desD* pseudogene, and on the opposite strand, upstream of *desE* is a *lysR* family transcriptional regulator (**Fig. 1c).** The DesA sequence from *A. desmolans* shares 81% amino acid (AA) identity with DesA from *C. scindens* and 90.5% AA identity with DesA from *Clostridium cadaveris*. The DesB from *A. desmolans* shares 83.3% AA identity with DesA from *C. scindens* and 89.8% AA identity with DesB from *C. cadaveris*.

Cortisol induces a broad transcriptional response in *A. desmolans*

To determine whether cortisol alters the physiology of *A. desmolans* beyond induction of steroid metabolism, we compared the transcriptomes of cells cultured in BHI containing 50 μM cortisol or vehicle (DMSO) (**Fig. 2a**). Cells were collected for RNA isolation and steroids were extracted from culture supernatants to confirm cortisol side-chain cleavage. The formation of 11β-OHAD (303 amu) was detected in all cortisol-treated cultures but not vehicle controls (**Fig. 2b**), confirming active cortisol metabolism under the conditions used for transcriptomic analysis. RNA-seq generated an average of approximately 35 million reads per sample, of which an average of 59.0% were assigned to annotated protein-coding genes. After quality control and differential expression analysis, multidimensional scaling separated cortisol-treated and vehicle-control samples by treatment, with consistent treatment-dependent expression patterns across biological replicates (**Supplementary Fig. 2a,b**).

Cortisol exposure produced extensive transcriptional remodeling in *A. desmolans*. Of the 2,784 genes encoded by the 2.75-Mb genome, 125 were significantly upregulated and 181 significantly downregulated using thresholds of |log2FC| > 1 and FDR < 0.05 (**Fig. 2c**). The most strongly induced genes belonged to the steroid-17,20-desmolase pathway responsible for cortisol side-chain cleavage, including *desA* (~250-fold), *desB* (~150-fold), *desE* (~300-fold), and *desD* pseudogene (~100-fold) **(Fig. 2c,d, Supplementary Table 1)**. Thus, genes directly associated with cortisol metabolism were among the strongest transcriptional responses to cortisol exposure.

Cortisol also altered expression of genes outside the steroid-metabolism locus. Three multidrug and toxic compound extrusion (MATE) family transporters (T363_RS0107930, T363_RS0107585, and T363_RS0110985) were significantly induced approximately threefold, identifying candidate transport systems potentially associated with steroid metabolism or the broader response to cortisol (**Fig. 2d, Supplementary Table 2**). Several genes encoding ferrous-iron transport proteins were similarly induced (**Supplementary Table 2**). Genes associated with flagellar assembly and export also exhibited coordinated

increases following cortisol exposure (**Fig. 2d, Supplementary Table 3**), suggesting that cortisol may influence bacterial motility.

In addition to these metabolic and motility-associated responses, cortisol exposure altered several transcriptional programs associated with bacterial adaptation to environmental stress. Genes involved in sporulation and genes annotated as prophage- or mobile genetic element-associated functions exhibited coordinated increases, although individual genes varied in statistical significance (**Fig. 2d, Supplementary Tables 4 and 5**). Eight genes associated with type II toxin–antitoxin systems were also significantly upregulated (**Fig. 2d, Supplementary Table 6**). Conversely, genes encoding numerous 30S and 50S ribosomal proteins and ATP synthesis-associated functions were downregulated, together with a nine-gene cluster associated with *de novo* purine biosynthesis (**Fig. 2d, Supplementary Tables 7-9**). Collectively, these findings indicate that the transcriptional response of *A. desmolans* to cortisol extends well beyond induction of steroid metabolism and is accompanied by changes in pathways associated with motility, persistence, mobile genetic elements, and energy-intensive biosynthetic processes.

Substrate specificity of recombinant *A. desmolans* DesAB

To characterize the catalytic properties of *A. desmolans* DesAB, initial-velocity kinetic constants were determined using a previously developed continuous enzyme-coupled assay (Devendran et al., 2018) in which the 17-ketosteroid product of DesAB-mediated side-chain cleavage was reduced by *C. lunatus* 17β-hydroxysteroid dehydrogenase (17β-HSDH), permitting DesAB activity to be monitored through NADPH consumption at 340 nm **(Fig. 3a,b)**. Recombinant DesAB (rDesAB) displayed Michaelis-Menten kinetics with cortisol, with a K_m of 45.9 ± 5.3 μM, V_{max} of 26.5 ± 1.4 nmol·mg^{-1} ·min^{-1}, k_{cat} of 3.6 min^{-1}, and catalytic efficiency (k_{cat}/K_m) of 0.078 min^{-1}·μM^{-1} **(Fig. 3c)**.

Substrate profiling revealed a strong preference of *A. desmolans* rDesAB for cortisol among the glucocorticoids examined. Relative to cortisol, 11-deoxycortisol retained 52.0 ± 1.3% activity, whereas cortisone displayed only 11.1 ± 0.28% activity (**Supplementary Fig. 3**), indicating that substitution at C11 substantially influences substrate utilization. LC-MS analysis also showed that *A. desmolans* rDesAB metabolized tetrahydrocortisol; however, we could not quantify its relative activity using the coupled assay because its side-chain-cleavage product is not a substrate for the 17β-HSDH coupling reaction (**Supplementary Fig. 3a-b**). Notably, tetrahydrocortisol was previously reported not to be metabolized by rDesAB from *Clostridium scindens* ATCC 35704 (Devendran et al., 2018).

Additional differences were observed between the recombinant DesAB (rDesAB) enzymes of *A. desmolans* and *C. scindens*. In contrast to *C. scindens* rDesAB, for which prednisone is a preferred substrate (Ly et al., 2020), *A. desmolans* rDesAB cleaved prednisone and dexamethasone only slowly: no product was detectable in the coupled assay or by LC-MS at 30 min, but side-chain cleavage was evident after 24 h (**Supplementary Fig. 3**). Both prednisone and dexamethasone are therefore poor substrates for the *A. desmolans* enzyme rather than non-substrates.

By contrast, corticosterone, 20α-dihydrocortisol, and 20β-dihydrocortisol were not substrates of *A. desmolans* rDesAB, consistent with previous observations for *C. scindens* rDesAB (**Supplementary Fig. 3**). Together, these results demonstrate that although DesAB-mediated glucocorticoid side-chain cleavage is conserved between these gut bacteria, the enzymes possess distinct substrate specificities.

Effects of 11β-hydroxyandrostenedione on gene expression in primary intestinal epithelial cells

Primary mouse intestinal epithelial cells (IECs) were treated with 0.5 μM 11β-OHAD, cortisol, or vehicle control (n = 6 per treatment) for 6 h, followed by collection of cells and culture

supernatants for RNA and protein analyses (**Fig. 4a**). Relative to vehicle-treated cells, 11β-OHAD significantly increased expression of 92 genes and decreased expression of 297 genes, using thresholds of |log2FC| > 0.58 and FDR < 0.05 (**Fig. 4b**). Pathway enrichment analysis of upregulated genes identified MAPK signaling as the most prominent enriched pathway, together with cytokine-cytokine receptor interactions, TNF, JAK-STAT and IL-17 signaling, cell-adhesion molecule interactions, and antigen processing and presentation (**Fig. 4c**).

Consistent with enrichment of MAPK signaling, 11β-OHAD significantly increased expression of several immediate-early and AP-1-associated genes, including *Fosb, Fosl1, Junb, Atf3,* and *Egr2*, as well as the MAPK feedback regulator *Dusp4* (**Fig. 4b**). Genes associated with adaptive oxidative-stress responses, including *Hmox1, Srxn1,* and *Sqstm1*, were also significantly increased. Notably, 11β-OHAD increased expression of *Csf1* and *Il34*, which encode the two ligands of CSF1R, together with *Csf1r* (**Fig. 4b**). Growth and repair-associated genes, including *Vegfa* and *Ereg*, were also significantly increased. *Vcam1* and *Icam1* expression increased but did not remain significant following correction for multiple comparisons. Conversely, pathway analysis of downregulated transcripts revealed enrichment of pathways associated with cell-cycle progression, DNA replication, and DNA repair. Together, these results demonstrate that 11β-OHAD induces a coordinated transcriptional shift characterized by increased stress-adaptive, cytokine-associated, and tissue-remodeling programs and decreased expression of proliferation-associated pathways in primary intestinal cells.

11β-OHAD alters cytokine and signaling protein abundance in primary intestinal epithelial cultures

To determine whether transcriptional changes induced by 11β-OHAD were accompanied by alterations at the protein level, culture supernatants were initially screened

using Proteome Profiler Mouse XL Cytokine Arrays. Based on this screen, vascular cell adhesion molecule 1 (VCAM1), insulin-like growth factor-binding protein 6 (IGFBP6), and colony-stimulating factor 1 (CSF1) were selected for quantitative analysis by ELISA (**Fig. 5a**). 11β-OHAD significantly increased VCAM1 secretion relative to vehicle control (Wilcoxon rank-sum test, $P = 0.024$), whereas IGFBP6 abundance was markedly decreased (Tukey's post hoc test, $P < 0.001$) (**Fig. 5b,c**). CSF1 secretion was also significantly increased following 11β-OHAD treatment (Wilcoxon rank-sum test, $P = 0.042$) (**Fig. 5d**). Consistent with the increased *Csf1r* transcript abundance observed by RNA-seq, CSF1R protein abundance was also significantly increased following 11β-OHAD treatment, as determined by immunoblotting and immunostaining (Tukey's post hoc test, $P < 0.005$) (**Fig. 5e-g**). Together, these protein-level changes support the transcriptional evidence that 11β-OHAD alters pathways associated with cellular stress responses, adhesion, growth-factor signaling, and cytokine-mediated communication.

Measurement of fecal *desA* abundance in a human cohort

We previously reported significantly higher hair cortisol concentrations among Black participants compared with non-Hispanic White participants in a Chicago cohort ($P < 0.0001$), with higher hair cortisol associated with residence in neighborhoods characterized by greater socioeconomic disadvantage and exposure to violent crime (Freiberg et al., 2020). As in our previous studies, the self-identified group labels are therefore used to describe unequal lived exposures and are not interpreted as biological categories. Because hair cortisol provides an integrated measure of longer-term cortisol exposure (Freiberg et al., 2020), we investigated whether the abundance of microbial genes encoding cortisol side-chain cleavage differed between these populations. Nucleotide sequences encoding *desA* from *A. desmolans*, *C. scindens*, and *C. cadaveris* were aligned and used to design and validate least degenerate qPCR primers targeting *desA* across these cortisol-metabolizing taxa (**Fig. S4**).

Fecal *desA* abundance was significantly higher in Black compared with non-Hispanic White participants (P = 0.045; **Fig. 6a**). Among participants with paired measurements, the association between hair cortisol and fecal *desA* abundance differed significantly by group (Fisher z, Z = 2.53, P = 0.011). Faecal *desA* abundance was positively and significantly associated with hair cortisol among Black participants (Spearman rho = 0.489, 95% CI 0.05 to 0.77, P = 0.035, n = 19) whereas a negative, non-significant association was observed among non-Hispanic White participants (rho = −0.274, 95% CI −0.59 to 0.12, P = 0.166, n = 27; **Fig. 6b**). These subgroup analyses were not pre-specified and both groups are small; the group-dependent pattern is reported as an observation requiring replication.

DISCUSSION

Cortisol elicited a far broader response in *A. desmolans* than the induction of steroid catabolism alone, and the steroid it generates is not biologically inert in host cells. Together, these observations recast microbial glucocorticoid metabolism as an exchange rather than a clearance step: the bacterium reads a host stress signal and returns a chemically distinct one. This study aimed to determine microbial endocrine effects between (1) host cortisol and the transcriptome of *A. desmolans,* (2) the products of cortisol side-chain cleavage by *A. desmolans* (11β-OHAD) on gene expression/protein levels in mouse intestinal epithelial cells, (3) the levels of *desA* in the stool of a Chicago human cohort that is stratified by hair cortisol, environmental stressors, and polyp formation.

Early studies demonstrated that an isolate of *A. desmolans* converts cortisol to 11β-OHAD (Bokkenheuser et al., 1986). Later work demonstrated that the genes *desA* and *desB* encode the enzymes responsible for cortisol side-chain cleavage (Devendran et al., 2018). However, transcriptional responses to environmental cortisol by *A. desmolans* have not been reported previously. The genes most upregulated in *A. desmolans* under *in vitro* cortisol induction were those in the steroid-desmolase pathway (*desABED*). Interestingly, an

annotated MFS transporter (WP_078097045.1) located in the same operon as *desABE* is a pseudogene of DesD. The upregulated DesD pseudogene in *A. desmolans* is only 108 amino acids (of the expected 475 amino acids) and contains high sequence similarity (98.1% and 70.3%) with the predicted DesD from *Intestinibacillus sp. Marseille*-P4005 and *Clostridium scindens* ATCC 35704, respectively. We identified several transporters upregulated in response to cortisol, which likely include glucocorticoid import and androgen export protein(s). Of note, several multidrug efflux transporters in the MATE family were upregulated. These transporters have been previously shown to have substrate specificity against other steroids, such as cholic acid, deoxycholic acid, and berberine (Kuroda & Tsuchiya, 2009). Biochemical characterization of these identified transporters will be needed to confirm their function. If the steroid importer and exporter are verified, obtaining crystal structures could lead to the development of novel inhibitors to block microbial androgen production *in vivo*.

We hypothesize that *A. desmolans* may respond to cortisol as a host-derived environmental signal, altering the expression of genes involved in motility and nutrient acquisition. Consistent with this possibility, cortisol exposure increased the expression of several genes encoding ferrous iron transport systems. Iron acquisition is important for bacterial growth and persistence in the gastrointestinal tract, where bioavailable iron can be limited. Studies in enteric bacteria have shown that disrupting iron acquisition systems, including both siderophore-mediated ferric uptake and ferrous iron transport, can impair intestinal colonization, although the magnitude of the effect depends on the host's inflammatory state and the available iron sources (Pi H et al, 2012; Stojilijkovic I et al, 1993). Thus, the cortisol-dependent induction of motility-associated genes and iron transport systems may reflect a coordinated transcriptional response that influences the ability of *A. desmolans* to adapt to the intestinal environment.

Additionally, several genes involved with motility, including flagellar synthesis and export, showed modest upregulation. Flagella-driven movement toward beneficial chemical gradients or away from toxic chemical gradients helps reposition cells to more favorable environments. Because synthesis of flagella is an energetic process, the benefits must outweigh the costs. Interestingly, *A. desmolans* significantly downregulates ATP synthase in the presence of cortisol, potentially suggesting that it is rerouting protons to motility, which is driven by proton motive force (Manson et al., 1977). It is well established that flagellar motility is an essential virulence factor for many enteric pathogens, which facilitate cellular invasion and translocation across the epithelium (Akahoshi & Bevins, 2022). There is currently no evidence that suggests *A. desmolans* is a pathogen; thus, flagella may simply be an important colonization factor for countering intestinal flow, reducing expulsion. Additional *in vitro* studies are needed to verify the phenotype and the function of the flagella. Importantly, these experiments will need to assess several strains of *A. desmolans,* as the originally isolated and characterized strain reports motility (Bokkenheuser et al., 1986)**,** whereas two other isolated strains do not (Ahn et al., 2016; Takada et al., 2016).

During times of stress, the host increases cortisol production from the adrenal cortex into circulation to regulate physiological functions, such as inflammation and immune response. As flagellin, a major structural component of the flagellar filament, is a ligand for TLR5, it can trigger pro-inflammatory responses in monocytes, fibroblasts, and epithelial cells (Duan et al., 2013). While we did not examine the combined effects of 11β-OHAD and/or 20β-dihydrocortisol and *A. desmolans* growth in co-culture with IEPs, methods have been previously developed that could be applied in future studies (Duan et al., 2013).

The cortisol-induced transcriptome of *A. desmolans* suggests that the cell may be responding to a host stress response in the form of increased luminal cortisol. Interestingly, there are several sporulation genes trending towards significant upregulation, which is in apparent contradiction to motility upregulation, as these are antagonistic functions. What this

result might rather suggest is bacterial population heterogeneity based on bulk-seq. Cortisol may be provoking a broad state-transition program rather than pushing cells towards one terminal fate. On the one hand, a sub-population may be eliciting a motile/foraging phenotype to seek a more favorable niche, while the other may be engaging in a persistence response in which active early sporulation circuitry is being expressed in cells that are committing to survival through dormancy. These results underscore the need to better understand the response of not only microbial communities, but also heterogeneity of responses within populations of strains to host signaling molecules and their microbial end-products.

Sequencing cortisol-induced transcriptomes of additional *desAB*-encoding and non-encoding microbes will allow us to gain a greater understanding as to why bacteria evolved and maintained cortisol metabolism. Comparisons among transcriptomes would reveal whether there is a universal microbial response to cortisol, or if the cellular response varies depending on the organism. Because the cortisol-induced transcriptome for *C. scindens* was sequenced more than 10 years ago (Ridlon et al., 2013), the experiment should be repeated for more robust and richer datasets. Because the depth of sequencing and number of replicates are so different, it is difficult to draw any comparative conclusions between the cortisol response in *A. desmolans* to *C. scindens*.

An important implication of these findings is that bacterial cortisol metabolism may represent more than the inactivation of a host glucocorticoid. Rather, microbial transformation of cortisol may alter the biological information conveyed by this host-derived signal. Exposure of primary intestinal cells to 11β-OHAD produced a coordinated transcriptional response characterized by MAPK/AP-1 and cytokine-associated signaling, adaptive stress responses, and genes involved in cellular adhesion and tissue remodeling, while pathways associated with cell-cycle progression and DNA replication were reduced. This response included significant induction of the immediate-early transcription factors *Fosb, Fosl1, Junb, Atf3,* and *Egr2*, together with induction of *Hmox1, Srxn1,* and *Sqstm1*, consistent with activation of

stress-adaptive signaling (Abdel-Latif et al., 2009; Fahrer et al., 2023). These transcriptional changes were accompanied by a marked increase in VCAM1 protein and a decrease in IGFBP6, further supporting remodeling of the cellular immune interface following exposure to 11β-OHAD (Li et al., 1997; Su et al., 2025). Thus, conversion of cortisol to 11β-OHAD does not appear to simply remove glucocorticoid activity, but instead generates a microbial steroid metabolite capable of eliciting a distinct host-cell response.

Particularly notable was the induction of the CSF1/IL-34-CSF1R axis. Both *Csf1* and *Il34*, which encode alternative ligands for CSF1R, were significantly increased following 11β-OHAD exposure, as was *Csf1r*, while increased CSF1 and CSF1R abundance was independently observed at the protein level. CSF1 and IL-34 participate in the maintenance and differentiation of tissue macrophage populations, raising the possibility that 11β-OHAD influences communication between intestinal cells and the local myeloid compartment. This possibility is especially intriguing in the intestine, where macrophages are positioned in close association with the epithelial compartment and participate in tissue homeostasis, repair, and inflammatory responses (Sun et al., 2024; Zwicker et al., 2015). Although CSF1R expression in the intestine is predominantly associated with myeloid populations, CSF1R upregulation in epithelial cells has been described in a variety of tissues as a molecular shift associated with tumorigenesis, tissue injury, and chronic inflammation. Whether the 11β-OHAD-driven increase in CSF1R observed in our primary intestinal cell preparations reflects a similar epithelial reprogramming event remains to be established (Ide et al., 2002; Lin et al., 2001; Menke et al., 2009; SAPI et al., 1998). Cell-type-resolved studies and functional perturbation of CSF1R signaling will therefore be required to determine whether this pathway contributes directly to the biological effects of 11β-OHAD.

The transcriptional response to 11β-OHAD also suggests that its effects should not be characterized simply as pro-inflammatory. Induction of MAPK/AP-1 and cytokine-associated pathways occurred together with genes associated with cytoprotection, growth-

factor signaling, and tissue repair, including *Hmox1, Vegfa,* and *Ereg (Liu & Fang, 2025)*. Conversely, pathways associated with DNA replication and cell-cycle progression were reduced. These observations are consistent with a transition from a proliferative state toward a stress-adaptive and tissue-remodeling phenotype (Kidane et al., 2014). Such a response could have consequences for epithelial barrier physiology and interactions with immune and stromal cells without necessarily representing overt inflammatory injury. Determining whether this response promotes mucosal adaptation, inflammation, repair, or different outcomes depending upon physiological context will require investigation in more complex intestinal models and in vivo.

Viewed together with the bacterial response to cortisol, these findings suggest a bidirectional form of host-microbe endocrine communication. Cortisol strongly induced bacterial genes responsible for its metabolism while also altering transcriptional programs associated with sporulation, motility, and mobile genetic elements, suggesting that this host glucocorticoid is accompanied by a broader change in bacterial physiology. The resulting steroid metabolite, 11β-OHAD, in turn altered intestinal cell signaling. We therefore propose that microbial cortisol metabolism can function as a form of endocrine signal transformation: a host-derived glucocorticoid associated with physiological stress is sensed and metabolized by members of the intestinal microbiota, generating a chemically distinct steroid capable of modifying host-cell physiology. In this model, microbial steroid metabolism does not merely terminate host signaling but may redirect it, providing a mechanism by which changes in host endocrine state could translate into altered microbial behavior and subsequently communicate back to the host.

To our knowledge, this is among the first comparisons of a validated biomarker of chronic HPA axis activity with the abundance of a defined microbial steroid-metabolising gene in humans (Freiberg et al., 2020). The group-dependent pattern we observe is not

readily explained by a simple model in which increased host cortisol exposure uniformly selects for cortisol-metabolising bacteria, though these exploratory subgroup analyses were not pre-specified, both groups are small, and the finding requires replication in larger independent cohorts before it can be interpreted. Its value lies less in what it establishes than in what it makes tractable: If microbial cortisol-metabolising capacity tracks host cortisol exposure differently across populations, then the sterolbiome's response to host endocrine signals is conditioned by factors beyond circulating glucocorticoid concentrations. Candidates include the composition and strain-level gene content of the microbial community, the expression rather than mere presence of desmolytic pathways, the quantity of cortisol actually delivered to the colon after host 11β-HSD activity and intestinal reabsorption, the co-occurring bile acid pool, and the physicochemical conditions of the intestinal microenvironment, including transit time, pH, and redox state. Repeated sampling within individuals, across a cohort, pairing cortisol exposure with microbial functional gene abundance and steroid metabolite profiling, would determine whether the signal transformation we characterise in vitro operates in the human gut. Such a design would also distinguish within-individual variation, which tracks the host's own fluctuating cortisol exposure, from the stable between-individual differences in metabolic capacity that would be expected to shape host physiology over the longer term.

METHODS

Bacterial strains and growth conditions

Agathobaculum desmolans ATCC 43058 was purchased from the American Type Culture Collection (ATCC, Manassas, VA). The microbe was grown in butyl rubber-stoppered, aluminum crimp-sealed culture tubes (18 by 150 mm; series 2048 [Bellco Glass, Inc., Vineland, NJ, USA]) containing anaerobic brain heart infusion (BHI) broth.

Growth experiments were initiated with a 10% inoculum of late log-/early-stationary-phase cultures into tubes of sterile BHI medium with sterile 23-gauge needles and 1-ml syringes. All inoculated tubes were incubated vertically without shaking and in the dark at 37°C; growth was measured over time as the optical density (OD) at 600 nm using a spectrophotometer (Spectronic Instruments, Inc., Rochester, NY, USA); the optical path width (inner diameter of culture tubes) was 1.6 cm. Uninoculated culture media served as references. All conditions (50 μM cortisol or DMSO) were grown with 8 biological replicates, 4 replicates for RNA sequencing, and 4 extra replicates for storage in -80°C for quantitative reverse transcription-PCR (qRT-PCR).

Upon reaching mid-log phase, cells were transferred to ice, rapidly pelleted at 4°C, immediately flash-frozen, and stored at −80 °C until ready for processing. The supernatant of each sample was saved to verify induction by detecting the formation of 11β-OHAD via LC/MS.

Scanning Electron Microscopy (SEM)

A. desmolans ATCC 43058 was incubated in TSB. Culture (10 mL) in log phase was pelleted, then mixed with Karnovsky's fixative (1 mL, 2% glutaraldehyde and 2.5% paraformaldehyde), vortexed, and then centrifuged at 4,000 x g for 5 min at 4°C to fix the bacterial isolates. Supernatant was discarded, and the pellet was washed 3 times and sent to Materials Research Laboratory Central Research Facilities (University of Illinois at Urbana-Champaign, Urbana, Illinois, United States) for imaging with the Hitachi S-4800 high-resolution scanning electron microscope.

***A. desmolans* DNA Isolation and Sequencing**

A 10 mL culture of *A. desmolans* was aliquoted into two 15 mL tubes and centrifuged at 7000 rpm for 2 min. The supernatant was removed, and the cell pellets were washed with 4 mL

TE buffer (10 mM TRIS, 1 mM EDTA, pH 7.6). This washing step was repeated three times. The final cell pellet was resuspended in 900 µL TE buffer and mixed thoroughly. Lysozyme (40 µL, 100 mg/ml; Sigma) was added, followed by incubation for 1 h at 37 °C. Proteinase K (100 µL, 10 mg/ml; Sigma) was then added to the samples, which were incubated for 30 min at 37 °C. Subsequently, 260 µL of 5% SDS was added, followed by an additional 30 min incubation at 37 °C. Total volume was adjusted to 1.5 ml with TE buffer. An equal 1.5 mL buffered phenol (pH 8) was added, and samples were then centrifuged at 4000 rpm for 2 min. The aqueous phase was transferred to a new tube. Phenol/chloroform/isoamyl alcohol (25:24:1) was added (2 mL), mixed gently by inversion, and centrifuged. The aqueous phase was collected. DNA was precipitated by adding 1/10 volume 3 M sodium acetate and 2 volumes of ice-cold ethanol, followed by incubation at -80 °C for 30 min. Samples were centrifuged at 13,600 xg for 30 min at 4 °C. The supernatant was discarded, and the DNA pellet was washed with 1 mL of 70% ethanol, followed by centrifugation at 13,600 xg for 30 min at 4 °C. After removal of the ethanol, the pellet was air-dried at room temperature and resuspended in 50 µL TE buffer. DNA concentration and purity were assessed using a spectrophotometer and submitted for sequencing (PlasmidSaurus, Louisville, KY).

Genome Sequencing and Assembly. The genome of *Agathobaculum desmolans* was sequenced using Oxford Nanopore long-read technology. Reads were quality-filtered using NanoFilt v2.8.0 with the parameters -q 10 -l 1000 --headcrop 50 --tailcrop 50 --maxlength 50000, yielding 16,892 reads. Reads were corrected using Canu v2.2 and assembled using Flye v2.9.2 with an estimated genome size of 2.6 Mb and eight threads. The initial assembly comprised two contigs, with a total length of 2,761,594 bp, an N50 of 2,753,494 bp, and an estimated mean coverage of 38×. The assembly was polished using Medaka v2.0.1 with the r1041_e82_400bps_sup_v4.3.0 model [Moss et al., 2020]. Genome completeness and contamination were estimated using CheckM v1.1.9 (Parks et al., 2015), and the recovery of

conserved orthologous genes was assessed using BUSCO v6.0.0 with the bacteria_odb12 lineage dataset (116 BUSCO groups) [Basdani et al., 2026].

Taxonomic Classification and Comparative Genomics. Taxonomic placement was determined using GTDB-Tk v2.3.0 with GTDB release 226 [Chaumeil et al., 2022]. Species identity was further assessed using FastANI v1.32 by comparing the assembly against 64 RefSeq genomes from the genus *Agathobaculum* available in NCBI [Jain et al., 2018]. The resulting ANI matrix was subjected to hierarchical clustering of rows and columns using Euclidean distance and complete linkage with the hclust function in R. The clustered matrix was visualized as a heatmap using ggplot2, and dendrogram coordinates were extracted using ggdendro to illustrate relationships among genomes [O'Flynn et al., 2015]. Sequence similarity between the assembly and its closest reference genome was visualized using Circoletto (https://bat.infspire.org/circoletto/) [Darzentas, 2010].

Genome Annotation and Functional Characterization

Genome annotation was performed using Prokka v1.14.6 [Seemann, 2014], and functional gene categories were assigned using eggNOG-mapper v2.1.12 [Cantalapiedra et al., 2021]. The distribution of functional categories was summarized using a bar plot generated with ggplot2. The smaller circular contig was investigated for a possible plasmid origin using geNomad v1.12.0 [Camargo et al., 2024] and MOB-suite v3.1.0 (Robertson and Nash, 2018). These tools were used to assess plasmid-like sequence features and the presence of recognizable plasmid-associated replication and mobilization markers.

Genome Visualization and Data Availability

A circular representation of the assembled genome was generated using the Proksee web server (https://proksee.ca/) [Grant et al., 2023]. The genome assembly and raw sequencing

data were deposited in the NCBI database under BioProject PRJNA1477078, with assembly accession JCDKAR000000000.

Bacterial RNA Isolation

Total RNA was recovered from cells following disruption by bead beating in the presence of acid phenol as previously reported (Ridlon et al., 2013). In brief, stored cells were dissolved in a lysis buffer (200 mM NaCl, 20 mM EDTA, and diethylpyrocarbonate-treated water) and transferred to 2-ml screw-cap bead-beating tubes (Sarstedt AG & Co. KG, Nümbrecht, Germany). Cells were washed with the same buffer and resuspended in 500 µl of lysis buffer. To each tube, 200 µl of zirconium beads, 210 µl of 20% SDS (Ambion, Thermo Fisher Scientific, Waltham, USA), and 1 ml of 5:1 acid phenol were added. Cells were disrupted on a Mini-BeadBeater (Biospec Products, Inc., Bartlesville, OK, USA) at maximum speed twice for 1 min, with tubes kept on ice in between treatments. The aqueous and phenol phases were separated by centrifugation at 5,000 rpm for 1 min, and the aqueous phase was transferred to a new tube and washed once with 1 mL of 5:1 acid-phenol. Nucleic acids in the aqueous phase were precipitated at −80 °C for 60 min by addition of 1/10 volume of 5 M ammonium acetate (Ambion), 1 µl of Glycoblue (Ambion), 1 µl of RNase inhibitor (New England Biolabs [NEB], Ipswich, MA, USA), and 1 volume of ice-cold isopropanol, followed by centrifugation at 13,600g for 30 min. Precipitated nucleic acids were treated with RNase-free Turbo DNase (Ambion) according to the manufacturer's instructions to remove contaminated genomic DNA. Total RNA was purified using a MEGAclear kit (Ambion) according to the manufacturer's instructions. RNA purity and integrity were checked spectrophotometrically by the A260/A280 ratio and by separating 16S and 23S rRNA on a 1% agarose gel, respectively.

Bacterial RNA-Seq Analysis

Stranded RNA-Seq libraries were constructed and sequenced at the DNA Services laboratory of the Roy J. Carver Biotechnology Center at the University of Illinois at Urbana-Champaign using a TruSeq Stranded RNA sample preparation kit (Illumina, San Diego, CA, USA). Briefly, total RNA was quantified by Qubit (Life Technologies, Grand Island, NY, USA) and checked for integrity on a 2% eGel (Life Technologies). Starting with 1 µg of RNA, rRNA was removed from the total RNA using a Ribo-Zero Magnetic Bacteria kit (Illumina, CA). First-strand synthesis was performed with a random hexamer and SuperScript II (Life Technologies). Double-stranded DNA was blunt ended, 3' end A-tailed, and ligated to unique dual-indexed adaptors. The adaptor-ligated double-stranded cDNA was amplified by PCR for 8 cycles with Kapa HiFi polymerase (Kapa Biosystems, Wilmington, MA, USA). The final libraries were quantified on Qubit, and the average size was determined on an AATI Fragment Analyzer (Advanced Analytics, Ames, IA, USA). Libraries were pooled evenly and cleaned to ensure removal of primer and adaptor dimers and then evaluated on an AATI Fragment Analyzer. The final pool containing 20 libraries was diluted to a 5 nM concentration and loaded onto one SP Flow cell lane and then sequenced on an Illumina NovaSeq, for a total single-read length of 100 base pairs.

Bioinformatics

Quality control of raw RNA-Seq reads was performed by using FastQC (V0.11.8) (Andrews, S. 2010). Reads that had mean FastQC quality scores of >35 were used for further analysis. Raw reads were trimmed using Trimmomatic (V0.38) (Andrews, 217 C.E.) and aligned with rRNA sequences prepared from the genome of *A. desmolans* ATCC 43058 using bowtie2 (V2.4.2) (Langmead & Salzberg, 2012) . Unaligned reads were saved and realigned with the indexed genome of *A. desmolans* ATCC 43058 (GenBank assembly accession: GCA_000701665.1) using bowtie2 (Langmead & Salzberg, 2012). Output SAM files containing the aligned reads were converted to name-sorted BAM files using Samtools

(V1.12) (Li et al., 2009) and were counted against a general transfer format (GTF) annotation of the genome using the featureCounts function of Subread (V2.0.0) (Liao et al., 2014) . Differential gene expression analysis was performed using edgeR and limma R packages (Ritchie et al., 2015; Robinson et al., 2010). A minimum *P* value of 0.05 was accepted as indicating differentially expressed genes. Gene expression (Benjamini and Hochberg corrected) was reported as $\log_2$FC with a cutoff of 1 (2-fold change) and a false discovery rate (FDR) cutoff of 0.05.

Cloning, expression, and purification of *A. desmolans desAB* genes in *E. coli*

DesA and *DesB* sequences from *A. desmolans* were codon-optimized for *E. coli* and synthesized into pET-IDT C His vector. The genes were constructed under the regulation of a single promoter with both *DesA* and *DesB* presenting *the E. coli* ribosome binding site, with DesB protein expressing the His-tag. The vector was transformed into BL21 *E. coli* cells and eventually overexpressed using IPTG as an inducer. Then, the cells were centrifuged for 40 min at 4000 rpm at 4℃, and the pellets were homogenized (AVESTIN EmulsiFlex C3 Homogenizer). DesA and DesB were purified using the TALON Metal Affinity Resin-gravity column. The proteins were washed with a binding buffer (50 mM Tris-HCl, pH 8.0, 500 mM NaCl, 35 µL/50mL 2-Mercaptoethanol) until no change of color in Bradford reagent was detected. Then protein was eluted (50 mM Tris-HCl pH 8.0, 500 mM NaCl, 250 mM imidazole, 35µl/50ml 2-Mercaptoethanol), 1.5ml fractions were collected, and protein purity was assessed using SDS-PAGE. The Bradford assay was performed to measure total protein concentration.

DesAB Characterization

DesAB activity was measured by the oxidation of NADPH at 340 nm (ε=6,220 $M^{-1}\cdot cm^{-1}$) using a coupled enzyme reaction with 17β-HSDH. The standard reaction mixture contained

50 mM MOPS buffer, pH 7.0, 1 μM $MnCl_2$, 5 μM TPP, 0.5 μM DesAB, 1 μM 17β-HSDH, 200 μM NADPH, and cortisol at different concentrations (5-200 μM) or 200 μM of different substrates, to a final volume of 0.2 ml. The reaction was initiated by the addition of rDesAB. Reactions were performed in a 96-well plate, and absorbance was measured continuously every 7 seconds for 25 min using the BioTek Epoch 2 plate reader (Agilent). Initial velocities were calculated from the linear portion of the absorbance versus time curves and plotted against substrate concentration. Kinetic parameters (K_m and V_{max}) were determined by fitting the data to the Michaelis-Menten equation using nonlinear regression in R. The relative velocity of the reaction was used to determine substrate specificity, compared to cortisol, which was set as 100%.

Steroid and Androgens Extraction

Following the enzymatic reaction, ethyl-acetate extraction was performed for further analysis of the substrates and products of the reaction. 1 mL of ethyl acetate was added to 0.5 mL of the reaction mixture, gently mixed by inversion, and set aside to allow phase separation. 500 μl of the upper organic layer was collected and evaporated under nitrogen gas. The dry residue was reconstituted in 500 μl methanol and analyzed by Liquid chromatography-mass spectrometry (LC-MS).

Whole-cell steroid bioconversion assays

For whole-cell steroid metabolism analysis, *A. desmolans* were grown under anaerobic conditions in TSB medium at 37 °C. After inoculation, cells were incubated with 50 μM of different steroid substrates for 24 h. 1ml of the reaction medium was removed and extracted using ethyl acetate as previously mentioned (Wang et al., 2025).

Liquid chromatography-mass spectrometry (LC-MS)

A Waters Acquity UPLC system coupled with a Waters Synapt G2-Si ESI mass spectrometer was used to perform the LC-MS analysis. Chromatographic separation was achieved on a Waters Acquity UPLC BEH C18 column (2.1 mm × 50 mm, 1.7 μm particle size) at a flow rate of 0.5 mL/min. The mobile phases consisted of 95% water, 5% acetonitrile (ACN), and 0.1% formic acid (FA) for eluent A and 95% ACN, 5% water, and 0.1% FA for eluent B. The gradient program was as follows: 0.0–0.5 min, 100% A; 0.5–6.0 min, linear decrease to 30% A and 70% B; 6.0–7.0 min, linear decrease to 0% A and 100% B; 7.0–8.0 min, 100% B; 8.1–10.0 min, return to 100% A for re-equilibration. The injection volume was 0.2 μl. This was performed at the UIUC Mass Spectrometry Laboratory.

Primary intestinal epithelial cell (IEC) isolation and treatments

Conventionally raised C57BL/6 mice (3M and 3F aged 8-12 weeks (IACUC protocol 23075) were euthanized by CO_2 asphyxiation; the small intestine was excised, cut longitudinally, and placed in ice-cold PBS for no longer than 10 min. The tissue was then minced into approximately 1-2 mm fragments and washed five times with 5 mL ice-cold PBS. The intestinal fragments were incubated in 10 mL of HBSS supplemented with 200 U/ml type 1 collagenase (ThermoFisher) and 100 U/ml hyaluronidase (Sigma-Aldrich) for 20 min at 37℃, with gentle inversion every 1-2 min. The dissociation solution was transferred to a new 15 mL tube and centrifuged at 100× g for 5 min at 4℃. The cell pellet was washed with 5ml DMEM containing 2% sorbitol and 2% FBS and centrifuged at 300× g for 5 min at 4℃. Cells were resuspended in complete medium (DMEM containing 10% FBS, 1% L-Gln, 1% Penicillin-streptomycin, 20mM HEPES, and 0.1U/ml insulin), plated in a 12-well plate at a density of approximately 200 crypts per cm^2, and incubated in 5% CO_2 at 37℃ for 90 min. After this initial incubation, the media containing non-adherent cells was transferred to a new 12-well plate. Culture medium was replaced after 24 h and subsequently every 24 h for 5 days. After 7-8 days of culture, cells were treated with 0.25% trypsin-EDTA for 1 min. Cells

were re-cultured up to one time before experimental treatments. 24 h before treatment, the culture medium was replaced with complete medium containing charcoal-stripped FBS (Gibco). Cells were then treated with 500 nM 11β-OHAD or vehicle control for 6 h. Following treatment, samples were collected for protein and RNA analysis, and culture supernatant was collected for cytokine secretion measurements.

IEC RNA extraction

Cells were lysed by adding 400 µl of TRI Reagent (Sigma-Aldrich) per well in a 12-well plate. Cells were scraped, and lysates were transferred to 1.5 mL microcentrifuge tubes. Chloroform (80 µl) was added to each sample, followed by vigorous mixing and incubation on ice for 10 min. Samples were then centrifuged at 12,000 ×g for 15 min at 4℃. The aqueous phase (200 µl) was transferred to a new tube and mixed with isopropanol (200 µl). After 10 min incubation on ice, RNA was precipitated by centrifugation at 12,000 × g for 15 minutes at 4℃. The supernatant was removed, and the RNA pellet was washed with 75% ethanol, followed by centrifugation at 12,000 × g for 10 minutes at 4℃. Residual ethanol was allowed to evaporate while the tubes remained open at room temperature for 3 min. The RNA pellet was resuspended in 40 µl of RNase-free water and treated with RQ1 DNase-1 (Promega, Madison, WI) for 15 min at room temperature. RNA was then cleaned using the GeneJet RNA purification kit (Thermo Fisher). RNA was quantified using Qubit 4 (ThermoFisher).

RNA-Seq Analysis of IECs

Total RNA samples from IEC samples were submitted to the Roy J. Carver Biotechnology Center, DNA Services Laboratory (University of Illinois at Urbana-Champaign, Urbana, Illinois, United States) for library construction and sequencing. Total RNAs were run on a Fragment Analyzer (Agilent) to evaluate RNA integrity. The total RNAs were converted into individually barcoded polyadenylated RNA-seq libraries with the Kapa HyperPrep mRNA kit

(Roche, CA), with prior removal of rRNAs with the FastSelect Bacteria kit (Qiagen, CA). Libraries were barcoded with Unique Dual Indexes (UDI's), which have been developed to prevent index switching. The adaptor-ligated double-stranded cDNAs were amplified with the Kapa HiFi polymerase (Roche). The final libraries were quantified with Qubit (ThermoFisher), and the average cDNA fragment sizes were determined on a Fragment Analyzer. The libraries were diluted to 10 nM and further quantified by qPCR on a CFX Connect Real-Time qPCR system (Biorad) for accurate pooling of barcoded libraries and maximization of the number of clusters in the flow cell. The barcoded RNAseq libraries were loaded on one SP lane on a NovaSeq 6000 for cluster formation and sequencing. The libraries were sequenced as single-read 100 nt reads. The fastq read files were generated and demultiplexed with the bcl2fastq v2.20 Conversion Software (Illumina, San Diego, CA) using default parameters. The quality of raw sequencing reads was assessed using FastQC, and sequencing quality metrics were summarized using MultiQC. Reads were quantified against the *Mus musculus* GRCm39 cDNA transcriptome obtained from Ensembl using Kallisto v0.51.0 (Bray et al., 2016). A Kallisto index was generated from the reference cDNA transcriptome. Transcript-level abundance estimates were imported into R using the tximport package with length-scaled TPMs and analyzed using the edgeR package (Chen et al., 2025; Robinson et al., 2010; Soneson et al., 2015). Differential gene expression analysis was performed using the limma-voom workflow (Law et al., 2014; Ritchie et al., 2015).

Network and pathway enrichment analysis

Differentially expressed genes with $|logFC| > 0.58$ and $FDR < 0.05$ were submitted to the STRING database (v12.0, string-db.org) using default settings (minimum interaction score: 0.4). The resulting interaction network was imported into Cytoscape (v3.10.2) for visualization, with node color mapped to logFC (red, upregulated; blue, downregulated). Gene Set Enrichment Analysis (GSEA) was performed using the clusterProfiler package

(v4.16.0) in R (v4.6.0). Genes were ranked by logFC and tested against mouse KEGG pathways (organism: mmu) using the gseKEGG function. Pathways with adjusted p-value < 0.05 (Benjamini–Hochberg correction) were considered significant.

Protein Extraction

Primary IEC culture was lysed using 400 µl lysis buffer (pH 7.8: 20mM Tris–HCl, 145mM NaCl, 5% glycerol, 1% Triton X-100, and Pierce Protease Inhibitor Mini Tablet (ThermoFisher) for 10ml buffer) per well, in a 12-well plate. Lysates were kept on ice during extraction. Subsequently, samples were centrifuged at 8,000 X g for 10 min; the supernatant was collected, and protein concentration was quantified using Bradford reagent.

Western Blot

Samples (50 µg total protein/lane for all proteins) were separated on 12% SDS-polyacrylamide gels. Following electrophoresis, proteins were transferred onto nitrocellulose membranes using a semi-dry transfer system (Trans-Blot Turbo, Bio-Rad). Membranes were blocked for 1 h at room temperature in TBST containing either 1% nonfat milk or 1% BSA. Blots were incubated overnight at 4°C with primary antibodies against CSF1R (Thermo Fisher Scientific, PA5-25974,1:500) and β-actin as a loading control (Cell Signaling Technology, #3700, 1:500). Membranes were washed three times with TBST and subsequently incubated for 1 h at room temperature with HRP-conjugated secondary antibodies: goat anti-rabbit IgG (Thermo Fisher Scientific, 31460, 1:500) or goat anti-mouse IgG (Thermo Fisher Scientific, 31430, 1:1000). Protein bands were visualized by enhanced chemiluminescence and imaged using the iBright CL750 Imaging System (Thermo Fisher Scientific). Band intensities were quantified by densitometric analysis using iBright Analysis Software (Desktop Version 5.4.0).

Immunostaining

12-well IEC culture plates were washed twice with PBS and fixed with 4% paraformaldehyde (400 µl per well) for 20 min at room temperature. Following fixation, cells were washed twice with a wash buffer (0.1% BSA in PBS) and permeabilized with 0.1% Triton X-100 in PBS (400 µl per well) for 20 min on ice. Cells were then blocked for 1 h in a blocking solution containing 1% goat serum and 1% BSA in PBS. Primary rabbit antibodies against CDX2 (Abcam, ab76541, 1:50) and CSF1R (Thermo Fisher Scientific, PA5-25974, 1:50) were diluted in blocking buffer (200 µl per well) and incubated with the samples for 1 h at room temperature. After primary antibody incubation, cells were washed twice with wash buffer and incubated with goat anti-rabbit Alexa Fluor 488 secondary antibody (Abcam, ab150077, 1:100, 200 µl per well) in blocking solution for 1h at room temperature in the dark. Following two washes with wash buffer, nuclei were counterstained with Hoechst 33342 (Thermo Fisher Scientific, H3569, 1:5000 in PBS, 300 µl per well) for 1 min. Cells were then washed once with PBS and once with double-distilled water. Fluorescence detection was performed using the ZOE Fluorescent Cell Imager (Bio-Rad).

Proteome Profiler Mouse Cytokine Array and ELISA

Cell culture supernatants were collected and centrifuged at 500 × g for 7 min at 4℃ to remove cell debris. For each treatment group, 100 µL from each biological replicate (n=6) was pooled to generate a single representative sample for cytokine profiling. The Proteome Profiler Mouse XL Cytokine Array (R&D Systems, ARY028) was used as an initial screening tool to identify differentially secreted factors and was performed according to the manufacturer's instructions. Membranes were imaged using the iBright CL750 Imaging System (Thermo Fisher Scientific). Candidate cytokines identified from the array were subsequently quantified by ELISA. Cell supernatants were diluted as follows: VCAM-1 (1:10), IGFBP-6 (1:2), and CSF1 (undiluted). ELISAs were performed using the Mouse VCAM-1 ELISA Kit (Thermo

Fisher Scientific, EMVCAM1), Mouse IGFBP-6 ELISA Kit (Thermo Fisher Scientific, EMIGFBP6), and Mouse M-CSF (CSF1) ELISA Kit (Thermo Fisher Scientific, EMCSF1), according to the manufacturer's instructions. Absorbance at 450 nm was measured using the Bio Tek Epoch 2 Microplate Reader (Alginat).

desA qPCR primer design and validation

Intestinal bacterial *desA* sequences were obtained from *Intestinibacillus* sp. Marseille-P4005 *desA* (DBQ51_RS07915), *C. scindens* ATCC 35704 *desA* (HDCHBGLK_RS04190), *C. scindens* S076 *desA* (HCEICBPK_RS01960), *C. scindens* SO77 *desA* (PBLEJBOC_RS0479), *A. desmolans desA* (AC4A7T_RS05035), *Clostridium cadaveris desA* (KQH81_RS10350). A ClustalOmega alignment was performed to identify the least degenerate regions from which to design oligos with equivalent T_m *and* amplicon length <150 bp. Oligos were designed using Integrated DNA Technology Inc. (IDT; Coralville, Iowa) PrimerQuest Tool. The following degenerate primers were obtained from IDT: desA_pangut_F 5'-TARAAGTATATGGYBTTTGATCCG-3' and desA_pangut_R 5'-GBAYATCCCAYTCATACATDCC-3'. We validated this primer set by running a melting curve with individual *desA*+ strain DNA and a DNA gel for the product, confirming the product is the expected size both in control DNA reactions and in patient DNA samples.

Human Cohort

Participants self-identifying as Black or White, aged 45–75 years, were enrolled at the time of screening or surveillance colonoscopy at Rush University Medical Center and the University of Illinois Chicago. Individuals were excluded if they had a current or recent malignancy, a history of colorectal cancer, major gastrointestinal disease, antibiotic use within the preceding months, regular use of prebiotics or probiotics, conditions or medications known to affect digestion, or were pregnant, nursing, or had recently menstruated.

Institutional review board approval was obtained from Rush University Medical Center (13102201), UIC/UIUC (2016-0495), and Purdue University (2022-1626), and written informed consent was obtained from all participants.

Stool collected approximately four weeks after colonoscopy was stored at −80 ℃. DNA was extracted with the DNeasy PowerSoil kit. Faecal pan-*desA* gene was quantified by SYBR Green qPCR relative to universal 16S rRNA gene primers using $2^{-\Delta Cq}$; primers are described in the previous section.

Statistics

Statistical analyses were performed in R (version 4.6.0). Data distributions were assessed with the Shapiro–Wilk test. Kinetic parameters (K_m and V_{max}) were determined by fitting data to the Michaelis-Menten equation using nonlinear regression. For IEC protein data, normally distributed data were analyzed by one-way ANOVA followed by Tukey's HSD post-hoc test; non-normally distributed data were analyzed by Kruskal-Wallis test with pairwise Wilcoxon rank-sum comparisons and Benjamini-Hochberg correction. For human cohort data, fecal *desA* abundance between racial groups was compared by two-sided Wilcoxon rank-sum test. Associations between hair cortisol and fecal *desA* abundance were assessed by Spearman rank correlation; 95% confidence intervals for rho were estimated by Fisher z-transformation. Differences in Spearman correlation coefficients between self-identified groups were tested using the Fisher z-transformation comparison. Exact n, statistical tests, and definitions of centre and error bars are given in the corresponding figure legends.

Acknowledgements

J.M.R. would like to express gratitude to the Center for Advanced Study at Illinois for the financial support and protected time to pursue this work. We want to thank Alvaro Hernandez, Director of the DNA Services Facility at the Roy J. Carver Biotechnology Center at Urbana-

Champaign, and Christopher J. Fields, Director of High-Performance Biology Computing at the Roy J. Carver Biotechnology Center, for nucleic acid sequencing and bioinformatics assistance. We thank Furong Sun, Director of the Mass Spectrometry Laboratory at Urbana-Champaign for LC-MS analysis. All chemical structures were created with ChemDoodle. Figures were created in BioRender. This work was supported by grants from the National Institutes of Health R01GM145920 [J.M.R, H.R.G], R01GM134423 [J.M.R., A.J.S.], R01CA204808 [H.R.G., J.M.R., E.M., L.T-H], U54MD012523 [L.T-H., J.M.R., H.R.G]. J.M.R. was also supported by UIUC Department of Animal Sciences Matchstick grant and Hatch ILLU-538-916.

Author contributions

J.M.R. conceptualized and designed the overall research. Experiments were performed and analyzed by M.F., F.V.F., T.W., L.K.K, M.A., P.S.B., H.D., S.L.D., H.R.G., and A.J.S. Clinical studies were performed by S.G., L.R., A.H., N.K., S.J.K., and supervised by P. G. W., P.G., E.M., and L.T-H. The manuscript was written by J.M.R., M.F., and L.K.L. with input from all authors. All authors edited the manuscript and approved the final draft.

Competing interests

The authors declare no competing interests.

Data Availability

Genome and raw data were submitted to the NCBI database under the BioProject PRJNA1477078, accession number JCDKAR000000000. The bacterial RNA-seq data and IEC RNA-seq data have been deposited under BioProject accession PRJNA1543534.

REFERENCES

Abdel-Latif, M. M., Duggan, S., Reynolds, J. V, & Kelleher, D. (2009). Inflammation and esophageal carcinogenesis. *Current Opinion in Pharmacology*, *9*(4), 396–404. https://doi.org/10.1016/j.coph.2009.06.010

Ahn, S., Jin, T.-E., Chang, D.-H., Rhee, M.-S., Kim, H. J., Lee, S. J., Park, D.-S., & Kim, B.-C. (2016). *Agathobaculum butyriciproducens* gen. nov. sp. nov., a strict anaerobic, butyrate-producing gut bacterium isolated from human faeces and reclassification of *Eubacterium desmolans* as *Agathobaculum desmolans* comb. nov. *International Journal of Systematic and Evolutionary Microbiology*, *66*(9), 3656–3661. https://doi.org/10.1099/ijsem.0.001195

Akahoshi, D. T., & Bevins, C. L. (2022). Flagella at the Host-Microbe Interface: Key Functions Intersect With Redundant Responses. *Frontiers in Immunology*, *13*, 828758. https://doi.org/10.3389/fimmu.2022.828758

Andrews, S. (217 C.E.). *FastQC: A Quality Control Tool for High Throughput Sequence Data*. Https://Www.Bioinformatics.Babraham.Ac.Uk/Projects/Fastqc/.

Barnard, M., Quanson, J. L., Mostaghel, E., Pretorius, E., Snoep, J. L., & Storbeck, K.-H. (2018). 11-Oxygenated androgen precursors are the preferred substrates for aldo-keto reductase 1C3 (AKR1C3): Implications for castration resistant prostate cancer. *The Journal of Steroid Biochemistry and Molecular Biology*, *183*, 192–201. https://doi.org/10.1016/j.jsbmb.2018.06.013

Basdani, D., Zekkas, S., Kylonis, A., Tzimotoudis, D., Fakis, G., Felföldi, T., Márialigeti, K., & Boukouvala, S. (2026). De-novo assembly of 82 bacterial genomes using Nanopore sequencing and prediction of biosynthetic capacity. *Scientific Data*, *13*(1). https://doi.org/10.1038/s41597-026-07202-6

Bokkenheuser, V. D., Winter, J., Morris, G. N., & Locascio, S. (1986). Steroid desmolase synthesis by *Eubacterium desmolans* and *Clostridium cadavaris*. *Applied and Environmental Microbiology*, *52*(5), 1153–1156. https://doi.org/10.1128/aem.52.5.1153-1156.1986

Bray, N. L., Pimentel, H., Melsted, P., & Pachter, L. (2016). Near-optimal probabilistic RNA-seq quantification. *Nature Biotechnology*, *34*(5), 525–527. https://doi.org/10.1038/nbt.3519

Camargo, A. P., Roux, S., Schulz, F., Babinski, M., Xu, Y., Hu, B., Chain, P. S. G., Nayfach, S., & Kyrpides, N. C. (2024). Identification of mobile genetic elements with geNomad. *Nature Biotechnology*, *42*(8), 1303–1312. https://doi.org/10.1038/s41587-023-01953-y

Cantalapiedra, C. P., Hernández-Plaza, A., Letunic, I., Bork, P., & Huerta-Cepas, J. (2021). eggNOG-mapper v2: Functional Annotation, Orthology Assignments, and Domain Prediction at the Metagenomic Scale. *Molecular Biology and Evolution*, *38*(12), 5825–5829. https://doi.org/10.1093/molbev/msab293

Chaumeil, P.-A., Mussig, A. J., Hugenholtz, P., & Parks, D. H. (2022). GTDB-Tk v2: memory friendly classification with the genome taxonomy database. *Bioinformatics (Oxford, England)*, *38*(23), 5315–5316. https://doi.org/10.1093/bioinformatics/btac672

Chen, Y., Chen, L., Lun, A. T. L., Baldoni, P. L., & Smyth, G. K. (2025). edgeR v4: powerful differential analysis of sequencing data with expanded functionality and improved support for small counts and larger datasets. *Nucleic Acids Research*, *53*(2). https://doi.org/10.1093/nar/gkaf018

Darzentas, N. (2010). Circoletto: visualizing sequence similarity with Circos. *Bioinformatics (Oxford, England)*, *26*(20), 2620–2621. https://doi.org/10.1093/bioinformatics/btq484

Devendran, S., Méndez-García, C., & Ridlon, J. M. (2017). Identification and characterization of a 20β-HSDH from the anaerobic gut bacterium *Butyricicoccus*

desmolans ATCC 43058. *Journal of Lipid Research*, *58*(5), 916–925. https://doi.org/10.1194/jlr.M074914

Devendran, S., Mythen, S. M., & Ridlon, J. M. (2018). The *desA* and *desB* genes from Clostridium scindens ATCC 35704 encode steroid-17,20-desmolase. *Journal of Lipid Research*, *59*(6), 1005–1014. https://doi.org/10.1194/jlr.M083949

Devendran, S., Shrestha, R., Alves, J. M. P., Wolf, P. G., Ly, L., Hernandez, A. G., Méndez-García, C., Inboden, A., Wiley, J., Paul, O., Allen, A., Springer, E., Wright, C. L., Fields, C. J., Daniel, S. L., & Ridlon, J. M. (2019). *Clostridium scindens* ATCC 35704: Integration of Nutritional Requirements, the Complete Genome Sequence, and Global Transcriptional Responses to Bile Acids. *Applied and Environmental Microbiology*, *85*(7). https://doi.org/10.1128/AEM.00052-19

Duan, Q., Zhou, M., Zhu, L., & Zhu, G. (2013). Flagella and bacterial pathogenicity. *Journal of Basic Microbiology*, *53*(1), 1–8. https://doi.org/10.1002/jobm.201100335

Fahrer, J., Wittmann, S., Wolf, A.-C., & Kostka, T. (2023). Heme Oxygenase-1 and Its Role in Colorectal Cancer. *Antioxidants (Basel, Switzerland)*, *12*(11). https://doi.org/10.3390/antiox12111989

Freiberg, M., Wang, T., Rosa, R. S. de L., Osswald, A., Melo, M. C. R., Stouffer, D. G., Buobu, P. S., Welsh, C., Yang, L., Abdel-Hamid, A. M., Doden, H. L., Devendran, S., Pollet, R. M., Goldberg, S., Ray, L., Hamm, A., Kessee, N., Dai, H., Mythen, S. M., … Ridlon, J. M. (2020). Gut bacteria convert cortisol into a distinct host signalling molecule. https://doi.org/10.1101/2020.06.12.149468

Grant, J. R., Enns, E., Marinier, E., Mandal, A., Herman, E. K., Chen, C.-Y., Graham, M., Van Domselaar, G., & Stothard, P. (2023). Proksee: in-depth characterization and visualization of bacterial genomes. *Nucleic Acids Research*, *51*(W1), W484–W492. https://doi.org/10.1093/nar/gkad326

Ide, H., Seligson, D. B., Memarzadeh, S., Xin, L., Horvath, S., Dubey, P., Flick, M. B., Kacinski, B. M., Palotie, A., & Witte, O. N. (2002). Expression of colony-stimulating factor 1 receptor during prostate development and prostate cancer progression. *Proceedings of the National Academy of Sciences*, *99*(22), 14404–14409. https://doi.org/10.1073/pnas.222537099

Jain, C., Rodriguez-R, L. M., Phillippy, A. M., Konstantinidis, K. T., & Aluru, S. (2018). High throughput ANI analysis of 90K prokaryotic genomes reveals clear species boundaries. *Nature Communications*, *9*(1), 5114. https://doi.org/10.1038/s41467-018-07641-9

Kidane, D., Chae, W. J., Czochor, J., Eckert, K. A., Glazer, P. M., Bothwell, A. L. M., & Sweasy, J. B. (2014). Interplay between DNA repair and inflammation, and the link to cancer. *Critical Reviews in Biochemistry and Molecular Biology*, *49*(2), 116–139. https://doi.org/10.3109/10409238.2013.875514

Kuroda, T., & Tsuchiya, T. (2009). Multidrug efflux transporters in the MATE family. *Biochimica et Biophysica Acta*, *1794*(5), 763–768. https://doi.org/10.1016/j.bbapap.2008.11.012

Langmead, B., & Salzberg, S. L. (2012). Fast gapped-read alignment with Bowtie 2. *Nature Methods*, *9*(4), 357–359. https://doi.org/10.1038/nmeth.1923

Law, C. W., Chen, Y., Shi, W., & Smyth, G. K. (2014). voom: Precision weights unlock linear model analysis tools for RNA-seq read counts. *Genome Biology*, *15*(2), R29. https://doi.org/10.1186/gb-2014-15-2-r29

Li, H., Handsaker, B., Wysoker, A., Fennell, T., Ruan, J., Homer, N., Marth, G., Abecasis, G., Durbin, R., & 1000 Genome Project Data Processing Subgroup. (2009). The Sequence Alignment/Map format and SAMtools. *Bioinformatics (Oxford, England)*, *25*(16), 2078–2079. https://doi.org/10.1093/bioinformatics/btp352

Li, X. C., Jevnikar, A. M., & Grant, D. R. (1997). Expression of Functional ICAM-1 and VCAM-1 Adhesion Molecules by an Immortalized Epithelial Cell Clone Derived from the Small Intestine. *Cellular Immunology*, *175*(1), 58–66. https://doi.org/10.1006/cimm.1996.1050

Liao, Y., Smyth, G. K., & Shi, W. (2014). featureCounts: an efficient general purpose program for assigning sequence reads to genomic features. *Bioinformatics (Oxford, England)*, *30*(7), 923–930. https://doi.org/10.1093/bioinformatics/btt656

Lin, E. Y., Nguyen, A. V., Russell, R. G., & Pollard, J. W. (2001). Colony-Stimulating Factor 1 Promotes Progression of Mammary Tumors to Malignancy. *The Journal of Experimental Medicine*, *193*(6), 727–740. https://doi.org/10.1084/jem.193.6.727

Liu, Z., & Fang, Y. (2025). Wound healing and signaling pathways. *Open Life Sciences*, *20*(1). https://doi.org/10.1515/biol-2025-1166

Ly, L. K., Rowles, J. L., Paul, H. M., Alves, J. M. P., Yemm, C., Wolf, P. M., Devendran, S., Hudson, M. E., Morris, D. J., Erdman, J. W., & Ridlon, J. M. (2020). Bacterial steroid-17,20-desmolase is a taxonomically rare enzymatic pathway that converts prednisone to 1,4-androstanediene-3,11,17-trione, a metabolite that causes proliferation of prostate cancer cells. *The Journal of Steroid Biochemistry and Molecular Biology*, *199*, 105567. https://doi.org/10.1016/j.jsbmb.2019.105567

Lyte, M. (2016). Microbial Endocrinology in the Pathogenesis of Infectious Disease. *Microbiology Spectrum*, *4*(2). https://doi.org/10.1128/microbiolspec.VMBF-0021-2015

Manson, M. D., Tedesco, P., Berg, H. C., Harold, F. M., & Van der Drift, C. (1977). A protonmotive force drives bacterial flagella. *Proceedings of the National Academy of Sciences of the United States of America*, *74*(7), 3060–3064. https://doi.org/10.1073/pnas.74.7.3060

Menke, J., Iwata, Y., Rabacal, W. A., Basu, R., Yeung, Y. G., Humphreys, B. D., Wada, T., Schwarting, A., Stanley, E. R., & Kelley, V. R. (2009). CSF-1 signals directly to renal

tubular epithelial cells to mediate repair in mice. *Journal of Clinical Investigation*, *119*(8), 2330–2342. https://doi.org/10.1172/JCI39087

Moss, E. L., Maghini, D. G., & Bhatt, A. S. (2020). Complete, closed bacterial genomes from microbiomes using nanopore sequencing. *Nature Biotechnology*, *38*(6), 701–707. https://doi.org/10.1038/s41587-020-0422-6

O'Flynn, C., Deusch, O., Darling, A. E., Eisen, J. A., Wallis, C., Davis, I. J., & Harris, S. J. (2015). Comparative Genomics of the Genus *Porphyromonas* Identifies Adaptations for Heme Synthesis within the Prevalent Canine Oral Species *Porphyromonas cangingivalis*. *Genome Biology and Evolution*, *7*(12), 3397–3413. https://doi.org/10.1093/gbe/evv220

Pi, H., Jones, S.A., Mercer, L.E., Meador, J.P., Caughron, J.E., Jordan, L., Newton, S.M., Conway, T., & Klebba, P.E. (2012). Role of catecholate siderophores in Gram-negative bacterial colonization of the mouse gut. *PLoS One*, 7(11):e50020. doi: 10.1371/journal.pone.0050020.

Pretorius, E., Africander, D. J., Vlok, M., Perkins, M. S., Quanson, J., & Storbeck, K.-H. (2016). 11-Ketotestosterone and 11-Ketodihydrotestosterone in Castration Resistant Prostate Cancer: Potent Androgens Which Can No Longer Be Ignored. *PloS One*, *11*(7), e0159867. https://doi.org/10.1371/journal.pone.0159867

Ridlon, J. M. (2020). Conceptualizing the Vertebrate Sterolbiome. *Applied and Environmental Microbiology*, *86*(16). https://doi.org/10.1128/AEM.00641-20

Ridlon, J. M., Ikegawa, S., Alves, J. M. P., Zhou, B., Kobayashi, A., Iida, T., Mitamura, K., Tanabe, G., Serrano, M., De Guzman, A., Cooper, P., Buck, G. A., & Hylemon, P. B. (2013). *Clostridium scindens*: a human gut microbe with a high potential to convert glucocorticoids into androgens. *Journal of Lipid Research*, *54*(9), 2437–2449. https://doi.org/10.1194/jlr.M038869

Ritchie, M. E., Phipson, B., Wu, D., Hu, Y., Law, C. W., Shi, W., & Smyth, G. K. (2015). limma powers differential expression analyses for RNA-sequencing and microarray studies. *Nucleic Acids Research*, *43*(7), e47–e47. https://doi.org/10.1093/nar/gkv007

Robertson, J., & Nash, J. H. E. (2018). MOB-suite: software tools for clustering, reconstruction and typing of plasmids from draft assemblies. *Microbial Genomics*, *4*(8). https://doi.org/10.1099/mgen.0.000206

Robinson, M. D., McCarthy, D. J., & Smyth, G. K. (2010). edgeR: a Bioconductor package for differential expression analysis of digital gene expression data. *Bioinformatics (Oxford, England)*, *26*(1), 139–140. https://doi.org/10.1093/bioinformatics/btp616

SAPI, E., FLICK, M., RODOV, S., CARTER, D., & KACINSKI, B. (1998). Expression of CSF-I and CSF-I receptor by normal lactating mammary epithelial cells. *Journal of the Society for Gynecologic Investigation*, *5*(2), 94–101. https://doi.org/10.1016/S1071-5576(97)00108-1

Schiffer, L., Arlt, W., & Storbeck, K.-H. (2018). Intracrine androgen biosynthesis, metabolism and action revisited. *Molecular and Cellular Endocrinology*, *465*, 4–26. https://doi.org/10.1016/j.mce.2017.08.016

Seemann, T. (2014). Prokka: rapid prokaryotic genome annotation. *Bioinformatics (Oxford, England)*, *30*(14), 2068–2069. https://doi.org/10.1093/bioinformatics/btu153

Sie, C., & Tropini, C. (2026). Microbial regulation of stress-associated signaling molecules and its role in health and disease. *NPJ Biofilms and Microbiomes*, *12*(1). https://doi.org/10.1038/s41522-026-00932-w

Soneson, C., Love, M. I., & Robinson, M. D. (2015). Differential analyses for RNA-seq: transcript-level estimates improve gene-level inferences. *F1000Research*, *4*, 1521. https://doi.org/10.12688/f1000research.7563.2

Stojiljkovic, I., Cobeljic, M., & Hantke, K. (1993). *Escherichia coli* K-12 ferrous iron uptake mutants are impaired in their ability to colonize the mouse intestine. *FEMS Microbiol Lett,* 108(1):111-5. doi: 10.1111/j.1574-6968.1993.tb06082.x.

Su, M., Zhao, W., Jiang, H., Zhao, Y., Liao, Z., Liu, Z., Xu, M., Jiang, S., Wu, L., Yang, Y., Wang, Z., Zeng, Z., Fang, Y., Tang, C., Miller, C. L., Evans, P. C., Wang, L., Banach, M., Jo, H., & Weng, J. (2025). Endothelial IGFBP6 suppresses vascular inflammation and atherosclerosis. *Nature Cardiovascular Research*, *4*(2), 145–162. https://doi.org/10.1038/s44161-024-00591-0

Sun, X., Xu, L., Ma, S., Du, J., Gu, H., & Wang, J. (2024). CSF1 is expressed by the intestinal epithelial cells to regulate Mφ macrophages and maintain epithelial homeostasis and is downregulated in neonates with necrotizing enterocolitis. *BMC Pediatrics*, *24*(1), 608. https://doi.org/10.1186/s12887-024-05047-9

Takada, T., Watanabe, K., Makino, H., & Kushiro, A. (2016). Reclassification of *Eubacterium desmolans* as *Butyricicoccus desmolans* comb. nov., and description of *Butyricicoccus faecihominis* sp. nov., a butyrate-producing bacterium from human faeces. *International Journal of Systematic and Evolutionary Microbiology*, *66*(10), 4125–4131. https://doi.org/10.1099/ijsem.0.001323

Wang, T., Ahmad, S., Cruz-Lebrón, A., Ernst, S. E., Olivos Caicedo, K. Y., Jeong, Y., Binion, B., Mbuvi, P., Dutta, D., Fernandez-Materan, F. V, Breister, A. M., Tang, E., Lee, J. W., Kang, J. D., Harris, S. C., Ikegawa, S., Gaskins, H. R., Erdman, J. W., Yang, G., … Ridlon, J. M. (2025). An expanded metabolic pathway for androgen production by commensal bacteria. *Nature Microbiology*, *10*(5), 1084–1098. https://doi.org/10.1038/s41564-025-01979-9

Wylensek, D., Hitch, T. C. A., Riedel, T., Afrizal, A., Kumar, N., Wortmann, E., Liu, T., Devendran, S., Lesker, T. R., Hernández, S. B., Heine, V., Buhl, E. M., M D'Agostino, P., Cumbo, F., Fischöder, T., Wyschkon, M., Looft, T., Parreira, V. R., Abt, B., …

Clavel, T. (2020). A collection of bacterial isolates from the pig intestine reveals functional and taxonomic diversity. *Nature Communications*, *11*(1), 6389. https://doi.org/10.1038/s41467-020-19929-w

Zwicker, S., Martinez, G. L., Bosma, M., Gerling, M., Clark, R., Majster, M., Söderman, J., Almer, S., & Boström, E. A. (2015). Interleukin 34: a new modulator of human and experimental inflammatory bowel disease. *Clinical Science*, *129*(3), 281–290. https://doi.org/10.1042/CS20150176

Figure Legends

Fig. 1 | Genome of *Agathobaculum desmolans* ATCC 43058 and organisation of the steroid-17,20-desmolase locus. a, Circular representation of the polished 2,761,597-bp assembly generated with Proksee. Rings from outermost to innermost show mobile genetic elements classified by function (integration/excision, stability/transfer/defence, replication/recombination/repair), prophage regions, antibiotic-resistance determinants, CRISPR arrays and Cas clusters; predicted coding sequences and open reading frames on both strands; rRNA and tRNA genes; GC skew (+/−); and GC content. The chromosome-sized contig comprises 2,753,494 bp encoding 2,784 predicted protein-coding sequences, 12 rRNA genes, 66 tRNA genes and one CRISPR locus. Inset, scanning electron micrograph of *A. desmolans* cells; scale bar, 3 µm. **b**, Organisation of the steroid-17,20-desmolase locus. *desA* and *desB* encode the two subunits of steroid-17,20-desmolase, *desE* encodes an SDR-family NAD(H)-dependent 20β-hydroxysteroid dehydrogenase, and a LysR-family transcriptional regulator is encoded immediately downstream on the opposite strand. The upstream *desD* homologue is a pseudogene encoding a truncated product of 108 residues relative to the 475-residue full-length protein. Arrows indicate direction of transcription; the locus is not drawn to scale. **c**, Functional classification of predicted coding sequences by eggNOG-mapper, grouped by COG superclass. Bars show gene counts per COG category; 722 genes were assigned to metabolism, 619 to information storage and processing, 452 to cellular processes and signalling, and 731 were poorly characterised or unassigned.

Fig. 2 | Cortisol induces broad transcriptional remodelling in *A. desmolans*. a, Experimental design. *A. desmolans* ATCC 43058 was cultured anaerobically in BHI containing 50 µM cortisol or an equivalent volume of DMSO vehicle and harvested at mid-exponential phase (n = 4 biological replicates per condition for RNA-seq). **b**, Extracted-ion chromatograms of ethyl acetate extracts of culture supernatants, showing cortisol (*m/z* 365,

retention time 3.16 min) and 11β-hydroxyandrostenedione (11β-OHAD; *m/z* 303, retention time 3.88 min). 11β-OHAD was detected in all four cortisol-treated cultures and in none of the four vehicle controls, confirming side-chain cleavage under the conditions used for transcriptomics. **c**, Mean–difference (MA) plot of differential gene expression in cortisol-treated relative to vehicle-treated cultures. Each point represents one gene; red and blue indicate significantly up- and downregulated genes, respectively [|log2FC| > 1, FDR < 0.05], and horizontal lines mark $|\log_2 FC| = 1$. Genes of the steroid-desmolase locus are labelled. **d**, Summary of functional categories responding to cortisol. Point position indicates the mean $\log_2$ fold change of genes within each category, point size indicates the number of genes in the category, and fill indicates the percentage of genes in that category meeting FDR < 0.05. Differential expression was assessed with edgeR/limma using thresholds of $|\log_2 FC| > 1$ and Benjamini-Hochberg FDR < 0.05.

Fig. 3 | Recombinant *A. desmolans* DesAB cleaves the cortisol side chain and is assayed by a coupled reaction. a, Scheme of the continuous coupled assay. Recombinant DesAB (rDesAB) cleaves the C17-C20 bond of cortisol to yield 11β-OHAD, which is reduced at C17 by *Curvularia lunata* 17β-hydroxysteroid dehydrogenase (17β-HSDH) to 11β-hydroxytestosterone (11β-OHT) with stoichiometric oxidation of NADPH, monitored as loss of absorbance at 340 nm. **b**, SDS-PAGE of purified rDesAB and 17β-HSDH following TALON metal-affinity chromatography. **c**, Initial-velocity kinetics of rDesAB with cortisol. Reactions contained 500nM rDesAB in 50 mM MOPS pH 7.0, 1 μM $MnCl_2$, 5 μM thiamine pyrophosphate, 1 μM 17β-HSDH and 200 μM NADPH, with cortisol from 5 to 200 μM. The curve is a non-linear least-squares fit to the Michaelis-Menten equation. Data are mean ± s.d. of 4 independent reactions from 4 enzyme preparations. Kinetic parameters: K_m = 45.9 μM, V_{max} = 26.5 nmol/min/mg, k_{cat} = 3.6 min^{-1}, k_{cat}/K_m = 0.078 min^{-1} μM^{-1}.

Fig. 4 | 11β-OHAD reprograms gene expression in primary mouse intestinal cell cultures. a, Experimental design. Primary intestinal cells were isolated from the small intestine of C57BL/6 mice (3F, 3M), cultured for 7-8 days, switched to charcoal-stripped serum for 24 h, and treated for 6 h with 0.5 μM 11β-OHAD, 0.5 μM cortisol, or vehicle (n = 6 biological replicates per treatment). Cells and supernatants were collected for RNA, protein and secreted-factor analysis. Representative CDX2 immunofluorescence (green) with Hoechst nuclear counterstain (blue). Scale bars, 100 μm.**b**, Representative protein–protein interaction network constructed from differentially expressed genes identified by RNA-seq (|logFC| > 0.58, FDR < 0.05), using STRING (v12.0, string-db.org) and visualized in Cytoscape (v3.10.2). Node color indicates log fold-change (logFC; blue, downregulated; red, upregulated). Edges represent STRING-predicted protein interactions. Not all DEGs are shown. 11β-OHAD significantly increased expression of 92 genes and decreased expression of 297 genes ($|\log_2 FC| > 0.58$, FDR < 0.05). **c**, GSEA dot plot showing the top 10 KEGG pathways enriched among upregulated and downregulated genes in intestinal epithelial cells. Point size represents gene set size; color indicates adjusted p-value.

Fig. 5 | 11β-OHAD alters secreted and cellular protein abundance in primary intestinal cell cultures. a, Proteome Profiler Mouse XL Cytokine Array of culture supernatants. For each treatment, equal volumes from six biological replicates were pooled into a single sample; arrays were used as a qualitative screen to nominate candidates and are not replicated. Positions of IGFBP6, CSF1 and VCAM-1 are indicated. **b-d**, Quantification by ELISA of VCAM1 (**b**), IGFBP6 (**c**) and CSF1 (**d**) in culture supernatants. **e**, Densitometric quantification of CSF1R immunoblots normalised to β-actin. **f**, Representative CSF1R and β-actin immunoblots; lanes are vehicle, cortisol and 11β-OHAD. **g**, Representative CSF1R immunofluorescence (green) with Hoechst nuclear counterstain (blue) for each treatment. Scale bars, 100 μm. In **b-e**, bars show the mean, error bars show s.e.m., and individual

biological replicates are plotted as open circles (*n* = 4-6 per group). Normally distributed data (**c**, **e**) were compared by one-way ANOVA with Tukey's HSD post-hoc test. Non-normally distributed data (**b**, **d**) were compared by Kruskal–Wallis test with pairwise Wilcoxon rank-sum comparisons and Benjamini–Hochberg correction for multiple comparisons. Exact *P* values are shown.

Fig. 6 | Faecal *desA* abundance and its association with chronic cortisol exposure differ between participant groups. a, Relative fecal desA abundance in non-Hispanic White (n = 52) and Black (n = 62) participants, quantified by SYBR Green qPCR using degenerate primers targeting *desA* of *Agathobaculum desmolans*, *Clostridium scindens* and *Clostridium cadaveris*, and normalized to universal 16S rRNA gene abundance by the 2^-ΔCq method and expressed relative to the White group mean (set to 1). Boxes show mean ± s.e.m.; open circles are individual participants. Groups were compared by two-sided Wilcoxon rank-sum test. **b,** Relationship between hair cortisol concentration and fecal *desA* abundance in the subset of participants with paired measurements (Black participants n = 19, orange triangles; White participants n = 27, blue circles). Both axes are log~10~-scaled; solid lines are linear fits within each group, and the dashed line is the pooled fit across both groups, with shading indicating 95% confidence intervals. The association differed significantly between groups (Fisher r-to-z test comparing two independent Spearman correlations, Z = 2.53, P = 0.011). Within groups, Spearman's rho = 0.489 (95% CI 0.05 to 0.77, P = 0.035) for Black participants and −0.274 (95% CI −0.59 to 0.12, P = 0.166) for White participants. Spearman's rho is rank-based and unaffected by the axis transformation. This comparison was not pre-specified, and both groups are underpowered to detect associations of this magnitude. Source data are provided as a Source Data file.

Figure 1

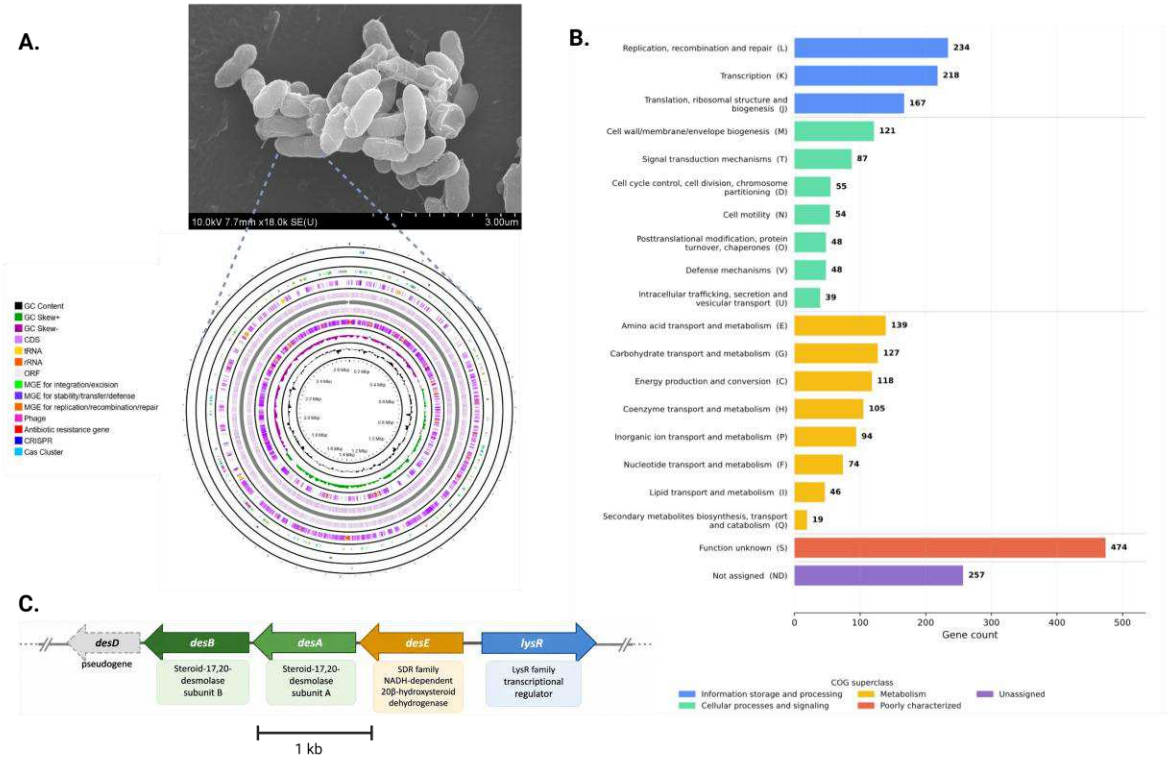

A.
10.0kV 7.7mm x18.0k SE(U)
3.00um
GC Content
GC Skew+
GC Skew-
CDS
tRNA
rRNA
ORF
MGE for integration/excision
MGE for stability/transfer/defense
MGE for replication/recombination/repair
Phage
Antibiotic resistance gene
CRISPR
Cas Cluster
B.
Replication, recombination and repair (L) 234
Transcription (K) 218
Translation, ribosomal structure and biogenesis (J) 167
Cell wall/membrane/envelope biogenesis (M) 121
Signal transduction mechanisms (T) 87
Cell cycle control, cell division, chromosome partitioning (D) 55
Cell motility (N) 54
Posttranslational modification, protein turnover, chaperones (O) 48
Defense mechanisms (V) 48
Intracellular trafficking, secretion and vesicular transport (U) 39
Amino acid transport and metabolism (E) 139
Carbohydrate transport and metabolism (G) 127
Energy production and conversion (C) 118
Coenzyme transport and metabolism (H) 105
Inorganic ion transport and metabolism (P) 94
Nucleotide transport and metabolism (F) 74
Lipid transport and metabolism (I) 46
Secondary metabolites biosynthesis, transport and catabolism (Q) 19
Function unknown (S) 474
Not assigned (ND) 257
0
100
200
300
400
500
Gene count
COG superclass
Information storage and processing
Cellular processes and signaling
Metabolism
Poorly characterized
Unassigned
C.
desD
pseudogene
desB
Steroid-17,20-desmolase subunit B
desA
Steroid-17,20-desmolase subunit A
desE
SDR family NADH-dependent 20β-hydroxysteroid dehydrogenase
lysR
LysR family transcriptional regulator
1 kb

Figure 2

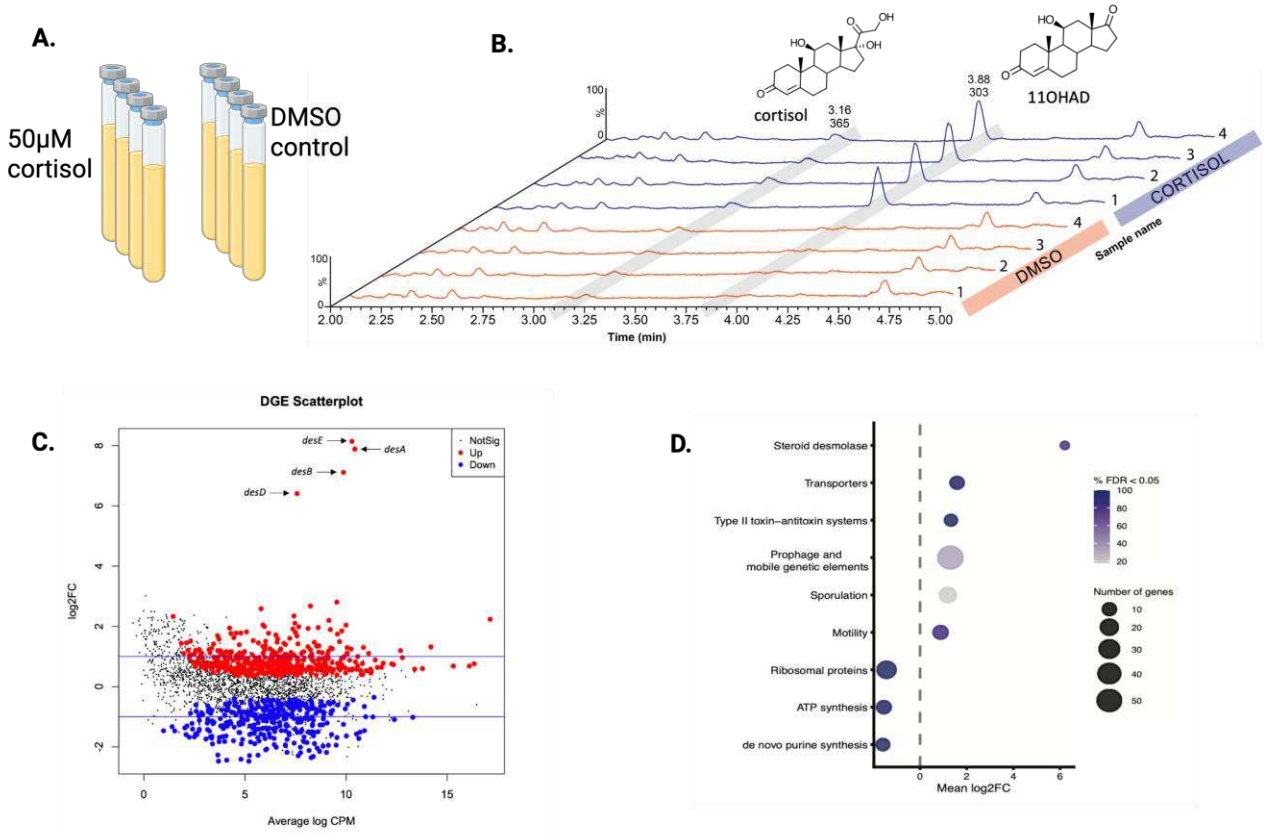

A.
50µM cortisol
DMSO control
B.
cortisol
3.16
365
11OHAD
3.88
303
Time (min)
CORTISOL
DMSO
Sample name
C.
DGE Scatterplot
NotSig
Up
Down
desE
desA
desB
desD
log2FC
Average log CPM
D.
Steroid desmolase
Transporters
Type II toxin–antitoxin systems
Prophage and mobile genetic elements
Sporulation
Motility
Ribosomal proteins
ATP synthesis
de novo purine synthesis
% FDR < 0.05
Number of genes
Mean log2FC

Figure 3

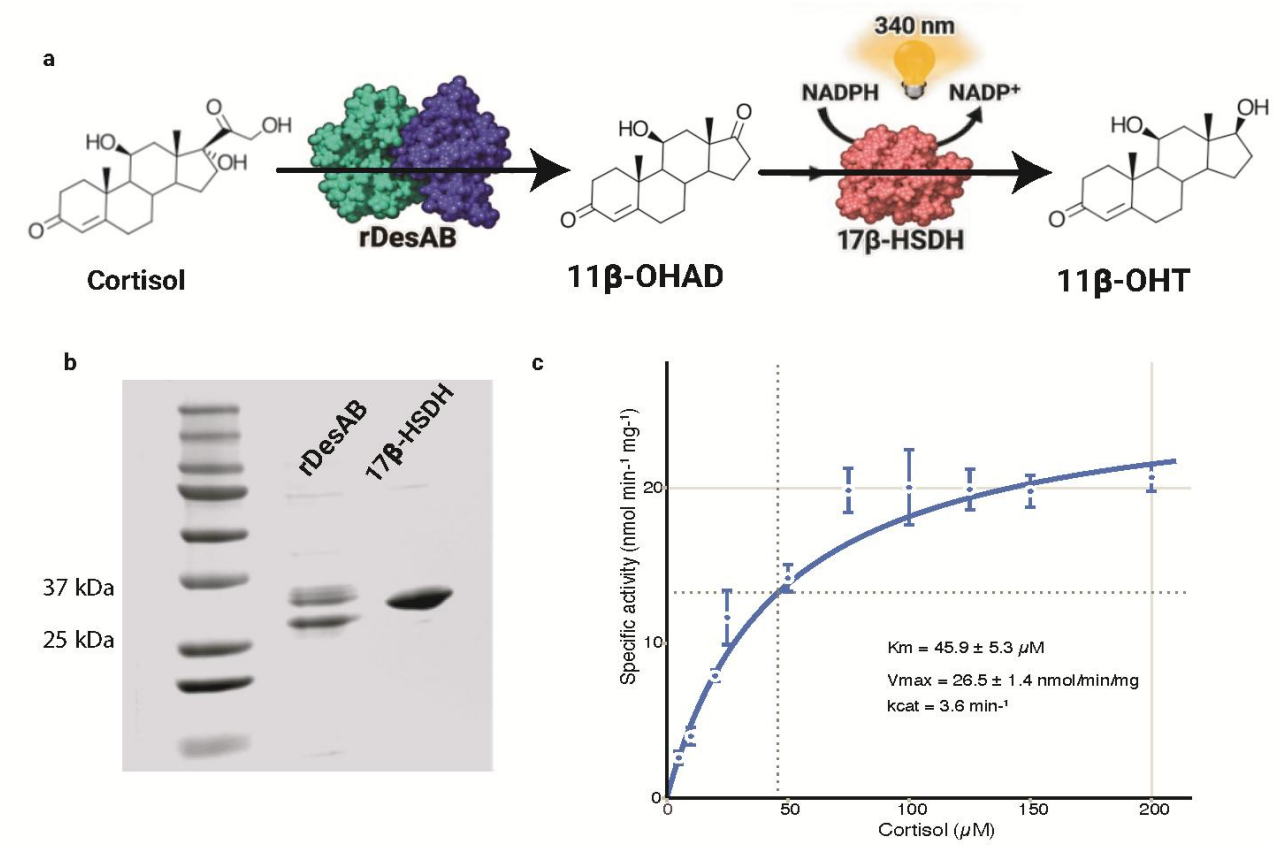


Figure 4

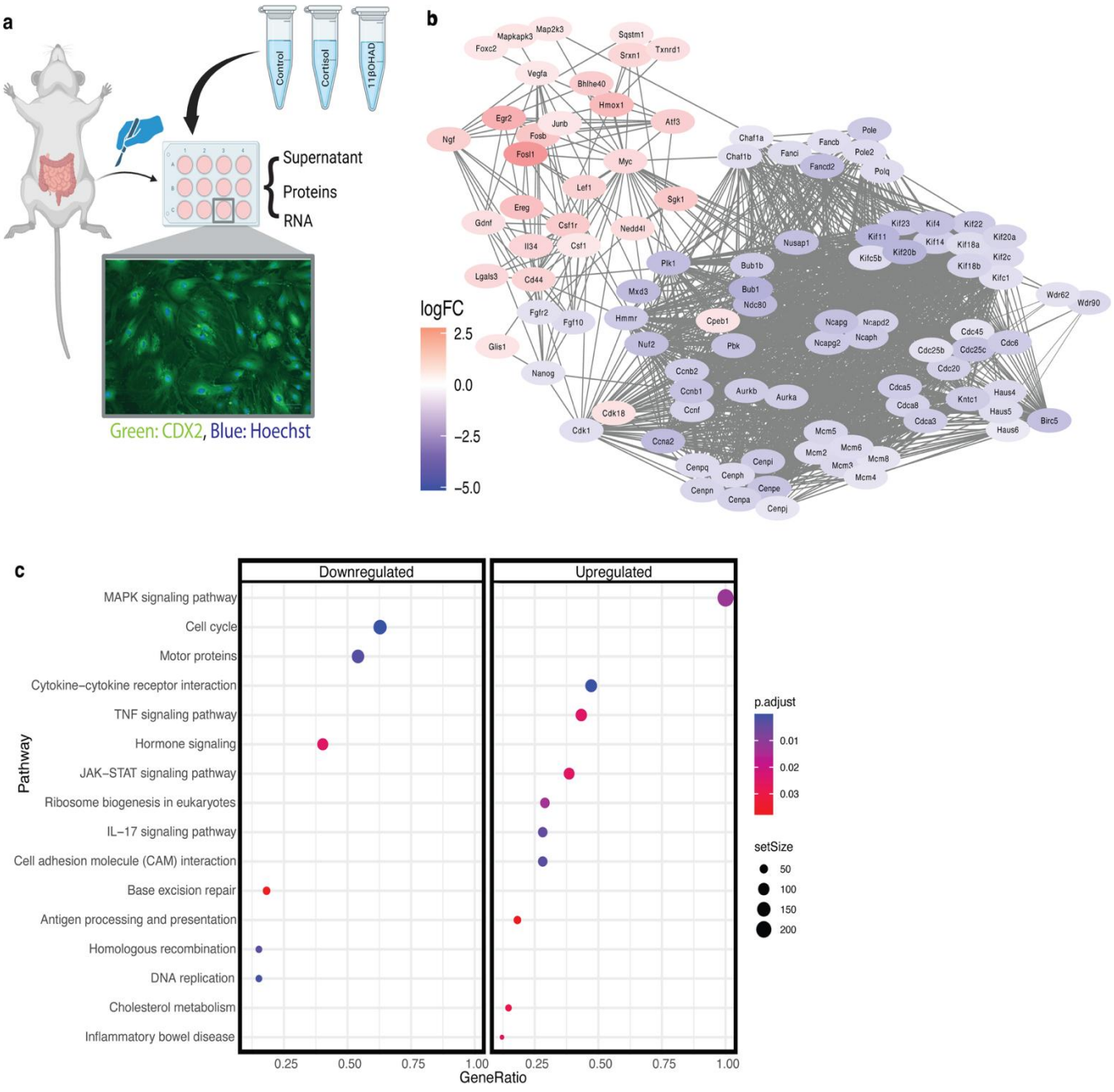

a
Control
Cortisol
11βOHAD
Supernatant
Proteins
RNA
Green: CDX2, Blue: Hoechst
b
logFC
2.5
0.0
−2.5
−5.0
c
Downregulated
Upregulated
MAPK signaling pathway
Cell cycle
Motor proteins
Cytokine−cytokine receptor interaction
TNF signaling pathway
Hormone signaling
JAK−STAT signaling pathway
Ribosome biogenesis in eukaryotes
IL−17 signaling pathway
Cell adhesion molecule (CAM) interaction
Base excision repair
Antigen processing and presentation
Homologous recombination
DNA replication
Cholesterol metabolism
Inflammatory bowel disease
Pathway
0.25
0.50
0.75
1.00
GeneRatio
p.adjust
0.01
0.02
0.03
setSize
50
100
150
200

Figure 5

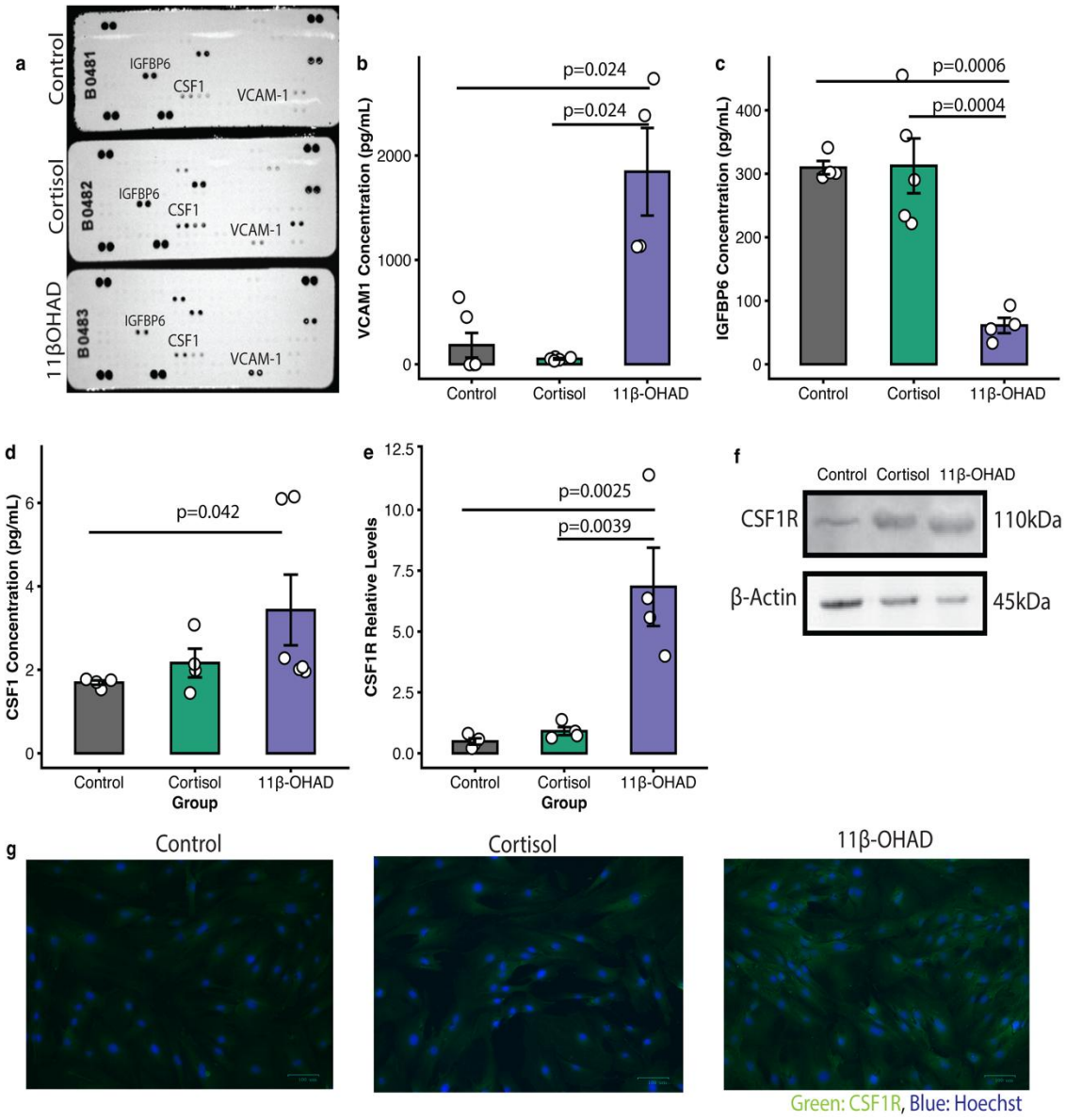
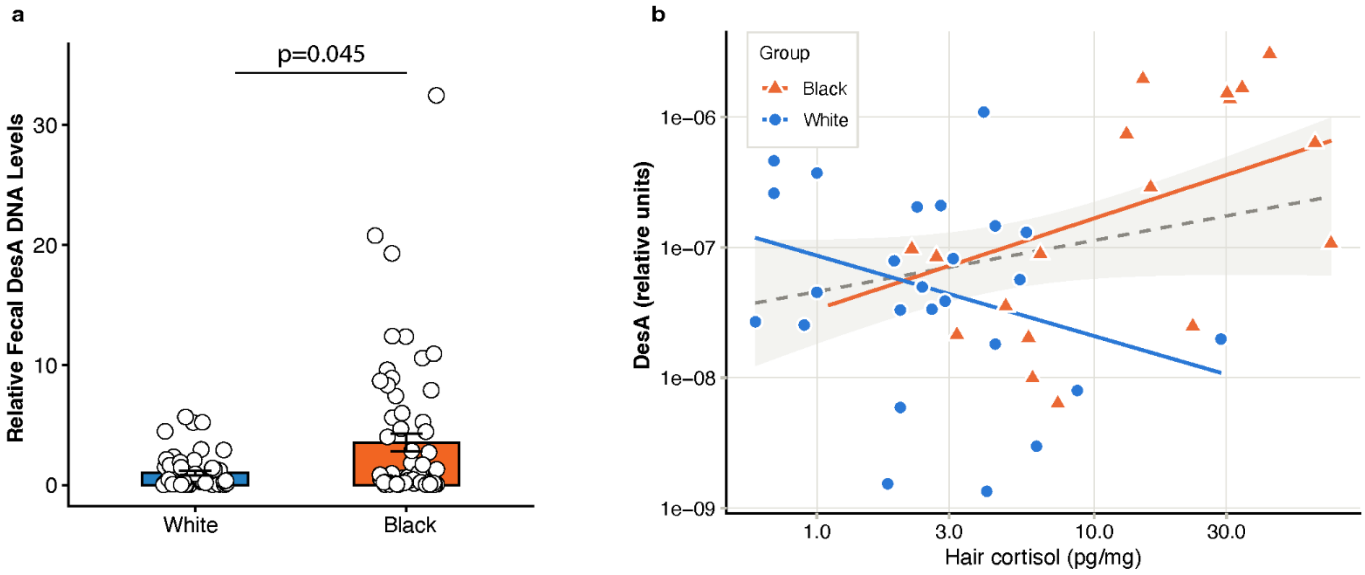

a
Control
Cortisol
11βOHAD
B0481
B0482
B0483
IGFBP6
CSF1
VCAM-1
b
VCAM1 Concentration (pg/mL)
p=0.024
p=0.024
Control
Cortisol
11β-OHAD
c
IGFBP6 Concentration (pg/mL)
p=0.0006
p=0.0004
d
CSF1 Concentration (pg/mL)
p=0.042
Group
e
CSF1R Relative Levels
p=0.0025
p=0.0039
f
CSF1R
β-Actin
110kDa
45kDa
g
Control
Cortisol
11β-OHAD
Green: CSF1R, Blue: Hoechst

Figure 6


a
p=0.045
Relative Fecal DesA DNA Levels
30
20
10
0
White
Black
b
Group
Black
White
1e−06
1e−07
1e−08
1e−09
DesA (relative units)
1.0
3.0
10.0
30.0
Hair cortisol (pg/mg)

Supplementary Files

This is a list of supplementary files associated with this preprint. Click to download.

- SupplementarydataA.desmolansV210.19.26.docx
- supplementaryfile.docx